

國立交通大學

電子工程學系 電子研究所碩士班

碩士論文

三模 MIMO 之無線區域網路
等化器設計



A Tri-mode MIMO Equalizer Design
for OFDM Based Wireless LANs

研究生：黃俊彥

Jun-Yen Huang

指導教授：溫瓊岸 博士

Dr. Kuei-Ann Wen

中華民國九十七年六月

三模 MIMO 之無線區域網路
等化器設計

A Tri-mode MIMO Equalizer Design
for OFDM Based Wireless LANs

研究生：黃俊彥

Student : Jun-Yen Huang

指導教授：溫瓊岸 博士

Advisor : Dr. Kuei-Ann Wen

國立交通大學

電子工程學系 電子研究所碩士班



Submitted to Department of Electronics Engineering & Institute of
Electronics

College of Electrical & Computer Engineering

National Chiao Tung University

in Partial Fulfillment of the Requirements

for the Degree of Master

in

Electronic Engineering

June 2008

中華民國九十七年六月

三模 MIMO 之無線區域網路 等化器設計

研究生：黃俊彥

指導教授：溫瓊岸博士

國立交通大學

電子工程學系 電子研究所碩士班

摘要

本論文提出一個可操作在具兩個傳送天線與兩個接收天線的三模等化器(Equalizer)。所提出的三模等化器，在高速的無線區域網路(Wireless LANs)中，可操作模式包含 SISO 模式、SDM-MIMO 模式和 STBC-MIMO 模式共三個模式。為考慮載波頻率偏移(Carrier Frequency Offset, CFO) 對系統的影響，本論文提出一個方法來有效率的減緩剩餘載波頻率偏移(Residual CFO)所造成的影響，以降低通道估測的錯誤。接著，提出一個高效率的載波頻率偏移追蹤器可以有效的降低系統封包錯誤率(Packet Error Rate)。

模擬結果顯示使用上述的方法可以在 2x2 多重輸入多重輸出(Multi-Input Multi-Output)的系統中，將剩餘載波頻率偏移對封包錯誤率的影響減低至 0.2dB 以內。考慮到實際的硬體實現，先觀察在三個模式中所使用演算法的相似度，在所提出的三模等化器架構中大量使用共用架構來減少面積消耗。最後，我們使用 FPGA 來實現所提出的電路。

A Tri-mode MIMO Equalizer Design for OFDM Based Wireless LANs

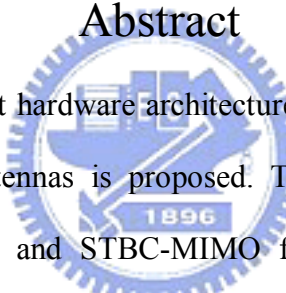
Student: Jun-Yen Huang

Advisor: Dr. Kuei-Ann Wen

Department of Electronics Engineering Institute of Electronics

National Chiao-Tung University

Abstract

The logo of National Chiao-Tung University is a circular emblem with a gear-like border. Inside the circle, there is a stylized building and the year '1896' at the bottom.

In this thesis, an efficient hardware architecture for tri-mode equalizer with two transmit and two receive antennas is proposed. The proposed tri-mode equalizer supports SISO, SDM-MIMO and STBC-MIMO for wireless LANs is designed. Considering the effects of carrier frequency offset (CFO), an effective CFO mitigation method is proposed to reduce the channel estimation error caused by residual CFO. Then, an effective CFO tracking algorithm is also proposed to enhance packet error rate (PER) performance.

Simulation results show that the proposed CFO mitigation and tracking algorithm can effectively suppress the PER performance loss due to residual CFO within 0.2 dB in the 2x2 multi-input multi-output (MIMO) system. For practical implementation, a lot of shared-architectures are utilized to reduce area consumption of the tri-mode equalizer by observing the similarity in the algorithms of the three modes. FPGA is used to implement our design.

誌謝

首先，第一個要感謝的是指導教授，溫瓊岸教授。感謝老師在兩年研究生涯中，不斷的給予俊彥指導與督促。溫老師的循循教誨，讓學生在學習訓練的路途上，能夠快速而正確的修正自己的研究方向，並且保持不鬆懈的心態進行研究。也感謝 TWT_LAB 在這兩年中提供的豐富研究資源，讓我在研究上無後顧之憂。另外，感謝各位口試委員們——李鎮宜教授與王晉良教授百忙中撥空提供寶貴的建議與指教，使得本論文更加的完整。

感謝實驗室的學長姐們的指導與照顧：嘉笙學長、文榮學長、哲生學長、文安學長、皓名學長、立協學長、懷仁學長、彥凱學長、建毓學長、翔琮學長及凱信學長等在研究上的意見與幫助。

感謝實驗室的同學們——柏麟、謙若、士賢、磊中、佳欣、國爵，二年來在課業和日常生活上總是相互的扶持與幫助。因為有你們，在趕進度的日子裡也能充滿歡笑，遇到困難時，大家都互相幫忙解決問題。同時也要感謝實驗室的助理們：苑佳、淑怡、慶宏、恩齊、智伶、嘉誠、宛君，幫忙實驗室裡大大小小的事，讓我們能更專心於研究。

最後，感謝默默支持我的家人及朋友。有你們的支持與分憂解勞，讓我可以無後顧之憂，全心的完成學業與研究，在此致上最深的感謝。

黃俊彥

2008

Contents

摘要	i
Abstract	ii
誌 謝	iii
Contents	iv
List of Figures	vi
List of Tables	viii
Chapter 1 Introduction	1
1.1 802.11n System Description	2
1.2 Channel Model	4
1.2.1 TGn channel model for 802.11n	5
1.2.2 Non-ideal effects	9
1.3 Organization of this thesis	12
Chapter 2 Equalizer Design for WLAN	13
2.1 System Platform Description	13
2.2 CFO Mitigation	15
2.3 Channel Estimation	19
2.4 Phase Error Tracking	21
2.4.1 Carrier Frequency Offset Tracking	22
2.4.2 Sampling Clock Offset Tracking	25
2.5.1 Zero Forcing channel equalizer for SISO mode	26
2.5.2 Maximal Likelihood STBC-MIMO Symbol Detection	29
Chapter 3 System Simulation and Performance Analysis	32

3.1 Design and Verification Flow.....	32
3.2 System Platform on MATLAB.....	33
3.3 Performance Analysis	34
3.3.1 Channel Estimation Accuracy Analysis	35
3.3.2 Phase Error Tracking Performance Analysis.....	36
3.3.3 System Performance	37
Chapter 4 Hardware Implementation	40
4.1 Common Architecture Design for Tri-mode Equalizer	40
4.2 Modules Design.....	41
4.2.1 CFO Mitigation Module Design	41
4.2.2 Channel Estimation Module Design	42
4.2.3 Phase Error Tracking Module Design.....	43
4.2.4 MIMO Detection Module Design.....	45
4.2.5 CORDIC Module Design.....	47
4.3 Implementation Results	49
4.3.1 Fixed-point Simulation.....	49
4.3.2 Hardware Synthesis.....	51
Chapter 5 Conclusions and Future Works	55
Bibliography	57
Vita	60

List of Figures

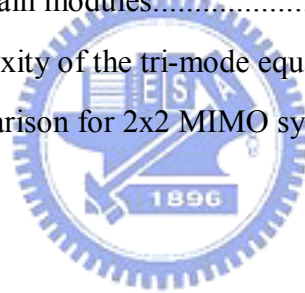
Figure 1.1: 802.11a/g and 802.11n preamble format.....	3
Figure 1.2: Baseband channel model.....	5
Figure 1.3: TGn channel model D delay profile	6
Figure 1.4: AOA (or AOD) of a Laplacian distribution, $AS = 30^\circ$	7
Figure 1.5: Carrier frequency offset effect.....	10
Figure 1.6: Mismatches between ADC/DAC sample frequencies	11
Figure 2.1: System block diagram.....	14
Figure 2.2: MIMO signal processing.....	14
Figure 2.3: Training symbols of 802.11n.....	15
Figure 2.4: The principle of D-symbol estimation.....	16
Figure 2.5: Training symbols required for proposed CFO mitigation.....	18
Figure 2.6: Smooth the estimated channels with a 3 taps fir filter.....	20
Figure 2.7: 2x2 MIMO Channel Estimation for 802.11n	20
Figure 2.8: 64QAM data constellation: (a) without PET (b) with PET.....	22
Figure 2.9: Constellation diagram of MMSE detection under different SNR	29
Figure 2.10: Constellation diagram of ML detection under different SNR.....	31
Figure 3.1: Design and verification flow	33
Figure 3.2: The system platform on MATLAB.....	33
Figure 3.3: Mean channel estimation errors vs. SNR under different CFO mitigation algorithms.....	35
Figure 3.4: Compare PET Algorithms at 2x2 MIMO, QPSK, $\frac{1}{2}$ Code rate	36
Figure 3.5: PER performance on STBC mode.....	38
Figure 4.1: Tri-mode equalizer architecture.....	40
Figure 4.2: The proposed CFO mitigation architecture.....	41
Figure 4.3: Tri-mode architecture of channel estimator	42

Figure 4.4: The proposed Tri-mode CFO tracker architecture.....	44
Figure 4.5: Tri-mode MIMO Detector architecture.....	46
Figure 4.6: The architecture of CORDIC cell at i-th stage	48
Figure 4.7: The architecture of CORDIC module	48
Figure 4.8: The normalized angle.....	49
Figure 4.9: Performance comparisons between floating point and fixed point simulation.....	50
Figure 4.10: The synthesis report of tri-mode equalizer on ISE	53
Figure 4.11: Comparison of RTL simulation and FPGA emulation.....	53
Figure 4.12: VeriComm and FPGA board.....	54



List of Tables

Table 1.1:	Physical layer related parameters	1
Table 1.2:	TGn channel model parameters.....	5
Table 1.3:	TGn channel model D parameters	8
Table 2.1:	Transmitted signals for 2x2 STBC-MIMO	30
Table 3.1:	PER Performance Comparison on SISO/SDM	37
Table 3.2:	System constraint for 802.11a and the required SNR to meet 10% PER for STBC-MIMO for 802.11n	39
Table 4.1:	Bit numbers of main modules.....	50
Table 4.2:	Hardware complexity of the tri-mode equalizer.....	51
Table 4.3:	Gate count comparison for 2x2 MIMO symbol detectors	51



Chapter 1

Introduction

Higher and higher data rates transmission are demanded for various multimedia applications in the wireless network. To increase the data rate and the robustness of transmission, the MIMO-OFDM technologies are first introduced in 802.11n wireless LAN system for various applications. IEEE 802.11n is developed based on IEEE 802.11a/g. The highest data rate can be outstandingly raised from 54Mbps to 600Mbps by using the additional antennas. The comparison of the physical layer related parameters are listed in Table 1.1. The differences between 802.11a/g and 802.11n include increasing the number of data sub-carriers, adding the optional 40MHz bandwidth operation, adding the 5/6 coding rate, and the optional half guard interval. All these adjustments are used to raise the maximum data transmission throughput.

Table 1.1 Physical layer related parameters

	802.11a/g	802.11n
Technology	SISO-OFDM	MIMO-OFDM
Bandwidth	20MHz	20MHz/40MHz
FFT size	64	64/128
Total number of subcarriers	52 (48 data subcarriers)	56/114 (52/108 data subcarriers)
Subcarrier spacing	312.5kHz	312.5kHz
Symbol interval	4 μ sec	4 μ sec
Coding rate	1/2 2/3 3/4	1/2 2/3 3/4 5/6
Max data rate	54Mbps	600Mbps

The distinct feature in baseband is the use of MIMO-OFDM technology. MIMO techniques can basically be classified into two groups: space division multiplexing (SDM) and space time coding (STC). SDM achieves a higher throughput by transmitting independent data streams on the different transmit branches simultaneously and at the same carrier frequency. On the other hand, STC increases the performance of the communication system by coding over the different transmitter branches. Space time block coding (STBC) is the STC technique indicated in 802.11n. STBC is first introduced by Alamouti [1], and is extended by Tarokh [2]. It has a main advantage of low complexity in hardware implementation.

Orthogonal frequency division multiplexing (OFDM) has been selected as the basis for several standards recently due to its advantages of dealing with multi-path outstandingly, reducing the complexity of equalizer, making single frequency possible, and high spectral efficiency. Further, Combining MIMO and OFDM technologies, MIMO-OFDM systems benefit from high throughput and high performance promising the future potential of the wireless networks.

1.1 802.11n System Description

In 802.11n, SDM-MIMO achieving high spectral efficiency is mandatory. STBC-MIMO which increases system performance is an optional robust transmission. Legacy SISO mode increasing the flexibility of usage are also supported by 802.11n. Conventionally, three different equalizers are used to decode the data from the three different modes, respectively. To utilize resources effectively and provide more flexibility of usage, a tri-mode equalizer supporting SISO, 2x2 SDM-MIMO and 2x2 STBC-MIMO for 802.11n applications is the design target.

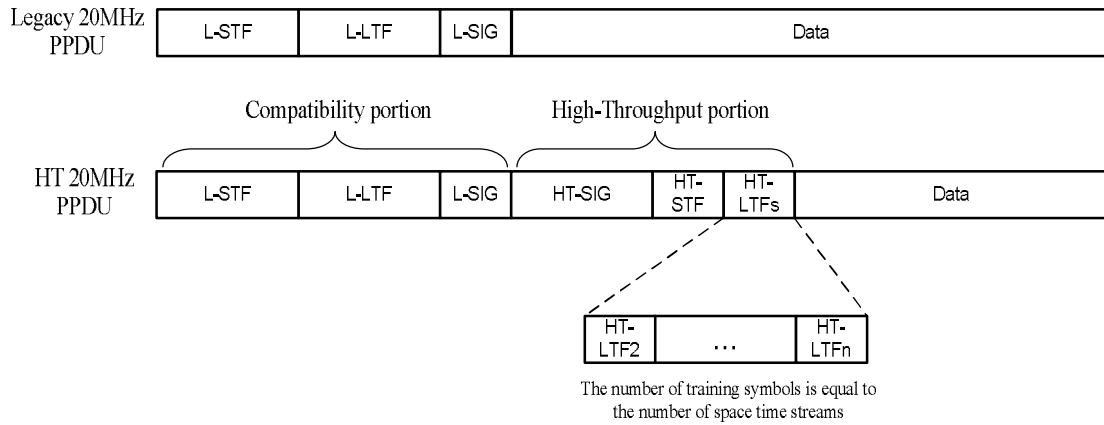


Figure 1.1 802.11a/g and 802.11n preamble format

The preamble in mixed-mode for 802.11n can be divided to two portions. In addition to new defined high-throughput portion, it concatenates the legacy preamble structure for 802.11a/g, i.e. compatibility portion. The reason is that the compatibility portion can be recognized by 802.11a/g systems, so this structure has the advantage of backward compatibility, and thus the flexibility of usage increases. We can realize the preamble structure clearly from Fig 1.1.

Similar to OFDM systems, MIMO-OFDM systems are very sensitive to phase errors. Even carrier frequency offset (CFO) estimation error (or residual CFO) shifts the sub-carrier frequencies and consequently introduces severe phase errors in OFDM. In addition, the accuracy of the channel estimation is also degraded by residual CFO, causing PER performance loss of the receiver. Accurate channel estimation is required to prevent inter-spatial stream interference (ISSI) in MIMO system particularly. Therefore, residual CFO must be estimated and compensated to ensure reliable communication with MIMO-OFDM.

With the repeated structure at legacy short training field (L-STF), autocorrelation-based techniques [3] at time domain are commonly used to estimate coarse CFO for practical implementation at receiver. The estimation errors left by coarse CFO estimation still cannot be neglected for system performance. In general,

with the repeated long preambles structure, i.e. L-LTF, an autocorrelation-based estimation [3] in time domain is utilized again for fine CFO estimation to determine the residue of the coarse CFO correction. After coarse and fine CFO estimation, we can get a satisfied performance in SISO mode for CFO reduction.

However, the channel estimation accuracy degraded by residual CFO for MIMO modes is still severe in 802.11n mixed-mode due to the large time lag between the L-LTF and the HT-LTFs which are used to estimate the MIMO channels [4]. Besides, while tracking the phase errors caused by CFO and SCO in the data portion, the existing pilot-based phase error tracking (PET) algorithms can not get a good performance against residual CFO due to few pilot numbers in wireless LANs.

In this study, a simple CFO mitigation method is proposed to help reduce the channel estimation error for mixed-mode in 802.11n by exploiting the structure of the packet preamble. Then an effective phase error tracking algorithm is also proposed to totally solve the CFO issues. We will demonstrate that with the proposed techniques, there is little loss due to CFO in system performance.

1.2 Channel Model

In this section, the channel model used for system simulation is introduced. In addition to the TGN proposed MIMO channel models [5], some non-ideal effects at receiver are added according to the TGN comparison criteria [6]. Non-ideal effects at receiver include additive white Gaussian noise (AWGN), CFO, and sampling clock offset (SCO). The baseband channel model used for simulation is illustrated as Fig 1.2. The TGN proposed channel models will be described in 1.2.1; the non-ideal effects will be introduced in 1.2.2.

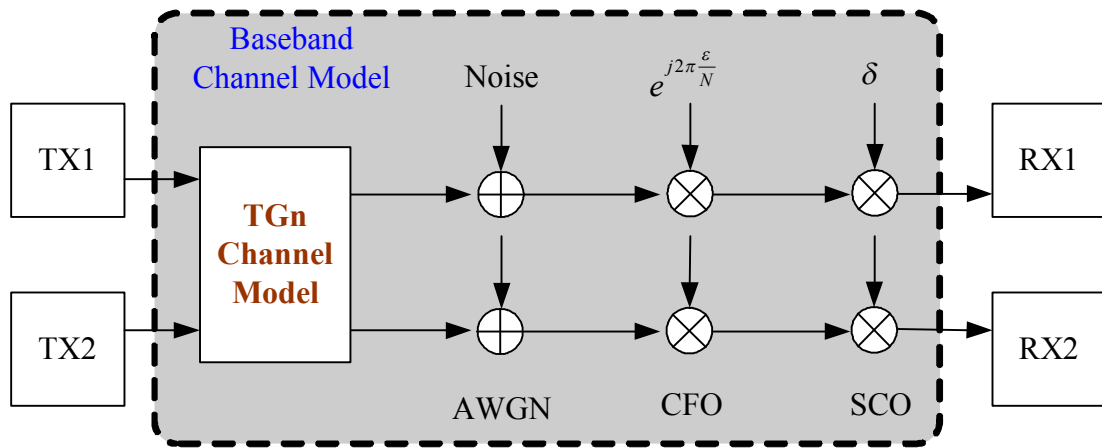


Figure 1.2 Baseband channel model.

1.2.1 TGn channel model for 802.11n

TGn classifies the indoor channel environments to six types and six models A-F are used to simulate the different channel conditions respectively. The sizes of environments increase from A to F. The parameters of channel models are listed in Table 1.2.

Table 1.2 TGn channel model parameters

Channel Model	RMS delay spread (ns)	Number of clusters	Number of taps
A	0	1	1
B	15	2	9
C	30	2	14
D	50	3	18
E	100	4	18
F	150	6	18

In the following, we briefly introduce the channel related parameters, and then explain how to develop MIMO channels.

(1) Power delay profile (PDP)

TGn channel models are built based on cluster model introduced firstly by Saleh and Valenzuela [7]. The average signal power of the k -th arrival within the l -th cluster is a Rayleigh-distributed random variable with a mean-square value that obeys a double exponential decay law:

$$\overline{\beta_{kl}^2} = \overline{\beta_{11}^2} e^{-T_l/\Gamma} e^{-\tau_{kl}/\gamma} \quad (1.1)$$

where T_l represents the arrival time of the l -th cluster, and τ_{kl} is the arrival time of the k -th arrival within the l -th cluster, relative to T_l . The parameters Γ and γ are time constants relative to environments. Fig. 1.3 shows the TGn channel model D delay profile.

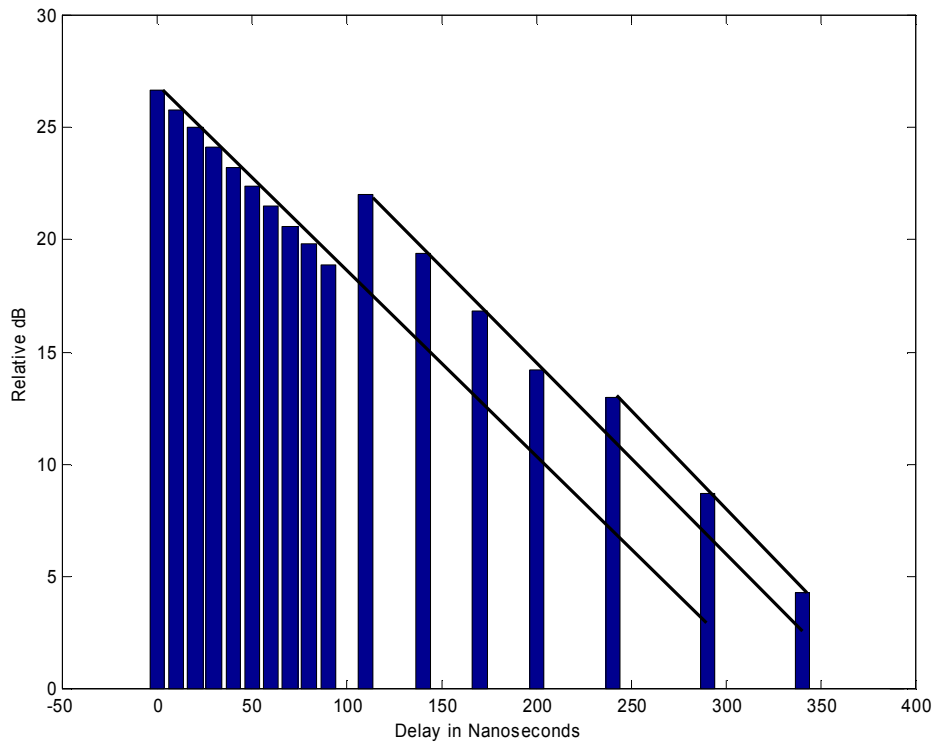


Figure 1.3 TGn channel model D delay profile.

(2) Power Angular Spread (PAS)

The angle of arrival statistics within a cluster were found to closely match the Laplacian distribution [8-10]

$$p(\theta) = \frac{1}{\sqrt{2}\sigma} e^{-|\sqrt{2}\theta/\sigma|} \quad (1.2)$$

where σ is the standard deviation of the PAS (which corresponds to the numerical value of angular spread; AS). The Laplacian distribution is shown in Fig 1.4 (a typical simulated distribution within a cluster, with AS = 30°).

Finally, the parameters of channel model D which is a typical office environment are listed in Table 1.3.

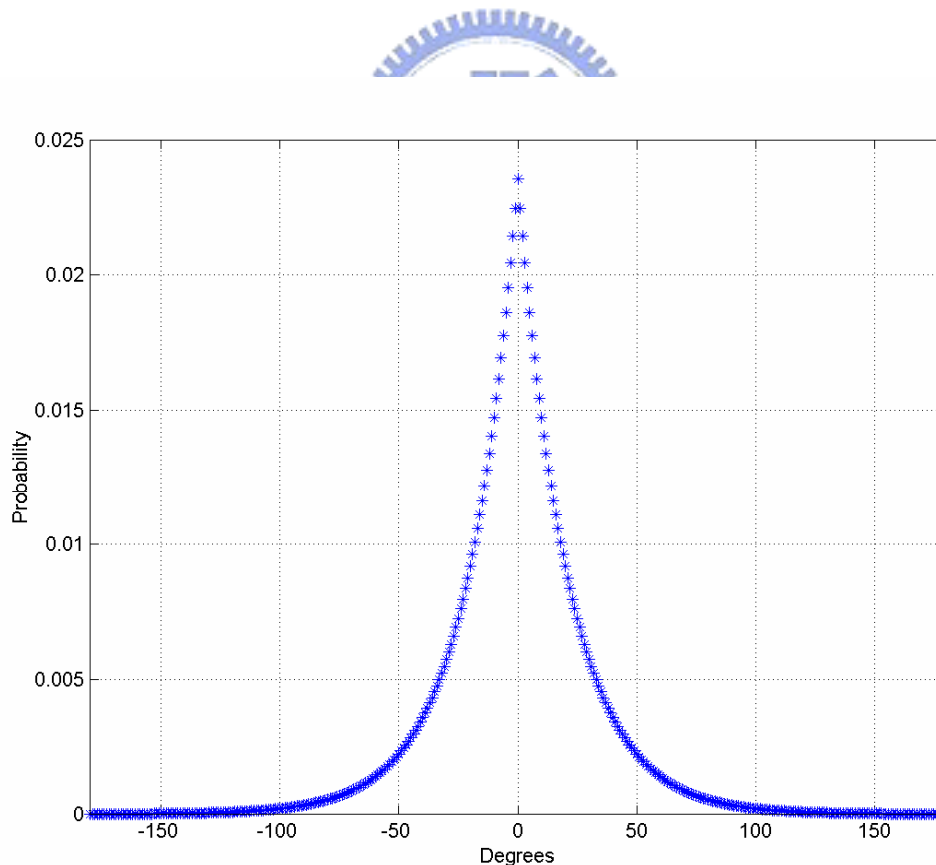


Figure 1.4 AOA (or AOD) of a Laplacian distribution, AS = 30°.

Table 1.3 TGN channel model D parameters.

Tap index		1	2	3	4	5	6	7	8	9	10	11	12	13	14	15	16	17	18			
Excess delay [ns]		0	10	20	30	40	50	60	70	80	90	110	140	170	200	240	290	340	390			
Cluster1	Power [dB]	0	-0.9	-1.7	-2.6	-3.5	-4.3	-5.2	-6.1	-6.9	-7.8	-9.0	-11.1	-13.7	-16.3	-19.3	-23.2					
	AoA [°]	158.9	158.9	158.9	158.9	158.9	158.9	158.9	158.9	158.9	158.9	158.9	158.9	158.9	158.9	158.9	158.9					
	AS (RX) [°]	27.7	27.7	27.7	27.7	27.7	27.7	27.7	27.7	27.7	27.7	27.7	27.7	27.7	27.7	27.7	27.7					
	AoD [°]	332.1	332.1	332.1	332.1	332.1	332.1	332.1	332.1	332.1	332.1	332.1	332.1	332.1	332.1	332.1	332.1	332.1				
	AS (TX) [°]	27.4	27.4	27.4	27.4	27.4	27.4	27.4	27.4	27.4	27.4	27.4	27.4	27.4	27.4	27.4	27.4	27.4				
Cluster2	Power [dB]											-6.6	-9.5	-12.1	-14.7	-17.4	-21.9	-25.5				
	AoA [°]											320.2	320.2	320.2	320.2	320.2	320.2	320.2				
	AS [°]											31.4	31.4	31.4	31.4	31.4	31.4	31.4				
	AoD [°]											49.3	49.3	49.3	49.3	49.3	49.3	49.3				
	AS [°]											32.1	32.1	32.1	32.1	32.1	32.1	32.1				
Cluster3	Power [dB]																		-18.8	-23.2	-25.2	-26.7
	AoA [°]																		276.1	276.1	276.1	276.1
	AS [°]																		37.4	37.4	37.4	37.4
	AoD [°]																		275.9	275.9	275.9	275.9
	AS [°]																		36.8	36.8	36.8	36.8



Using the PAS shape, AS, mean angle-of-arrival (AoA), and individual tap powers, correlation matrices of each tap can be determined as described in [11]. For the uniform linear array (ULA) the complex correlation coefficient at the linear antenna array is expressed as

$$\rho = \int_{-\pi}^{\pi} \cos(D \sin \phi) PAS(\phi) d\phi + j \int_{-\pi}^{\pi} \sin(D \sin \phi) PAS(\phi) d\phi \quad (1.3)$$

where $D = 2\pi d / \lambda$, and d is the distance between the two receiving antennas.

To correlate the X_{ij} elements of the matrix X , the following method can be used:

$$[X] = [R_{rx}]^{1/2} [H_{iid}] [R_{tx}]^{1/2} \quad (1.4)$$

where R_{tx} and R_{rx} are the receiving and transmitting correlation matrices, respectively, and H_{iid} is a matrix of independent zero mean, unit variance, complex Gaussian random variables, and

$$\begin{aligned} [R_{tx}] &= [\rho_{txij}] \\ [R_{rx}] &= [\rho_{rxij}] \end{aligned} \quad (1.5)$$

where ρ_{txij} are the complex correlation coefficients between i -th and j -th transmitting antennas, and ρ_{rxij} are the complex correlation coefficients between i -th and j -th receiving antennas. TGN also provide a MATLAB program [12] to generate correlated MIMO channels based on the above processes.

1.2.2 Non-ideal effects

(1) Additive White Gaussian Noise (AWGN)

AWGN is a complex Gaussian distributed variable in equivalent baseband channel model. It is zero mean and has the variance $\sigma^2 = N_0 / 2$, where $N_0 = E_s / SNR$, and E_s is defined as the average energy of one OFDM symbol.

(2) Carrier Frequency Offset (CFO)

CFO is caused by the frequency mismatch between the oscillator of transmitter and receiver. The signal x_n first up converts then down converts can be express as:

$$\begin{aligned}
 r_n &= x_n e^{j(2\pi f_t nT)} e^{-j(2\pi f_r nT)} \\
 &= x_n e^{j(2\pi (f_t - f_r) nT)} \\
 &= x_n e^{j(2\pi (\Delta f) nT)}
 \end{aligned} \tag{1.6}$$

where f_t and f_r are the frequencies of oscillator at transmitter and receiver respectively. Therefore, this will cause a common spectrum shift according to equation (1.6). In OFDM system, the orthogonality will be destroyed and then inter carrier interference (ICI) induced. Fig. 1.5 shows the effect of CFO in frequency domain.

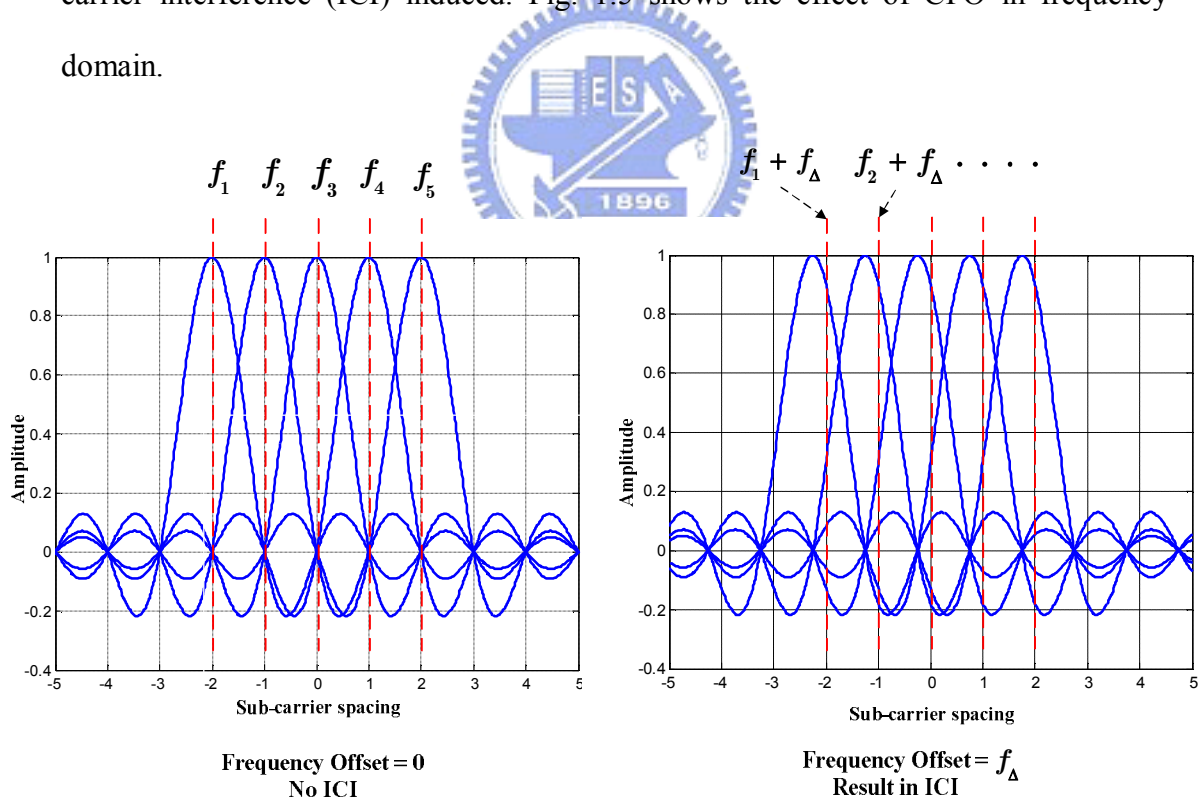


Figure 1.5 Carrier frequency offset effect

(3) Sampling Clock Offset

SCO is caused by the mismatch between ADC/DAC sampling frequencies, as

illustrated in Fig 1.4.

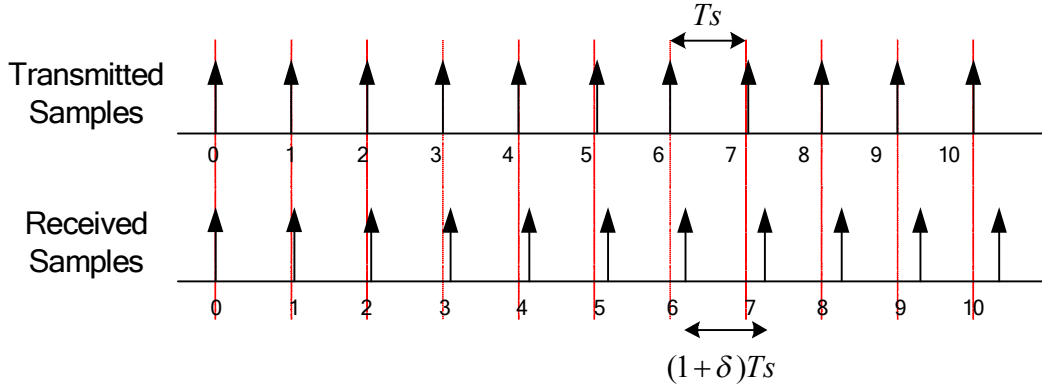


Figure 1.6 Mismatches between ADC/DAC sample frequencies.

Assume T_s is the transmitted sampling period, δ is the sampling clock offset value, and $(1+\delta)T_s$ is the received sampling period. In frequency domain, SCO enlarging or narrowing the spectrum in horizontal destroys the orthogonality in OFDM, thus it also induces ICI in OFDM systems.

To simulate the shifted signals, we interpolate the received signal using raised cosine filter.

$$h_{\text{interp}}(\tau) = \frac{\cos(\alpha(n+\tau))}{1 - (2\alpha(n+\tau)/\pi)^2} \text{sinc}(n+\tau) \times w(n+N), \quad n = -N/2, \dots, N/2 \quad (1.7)$$

where α is the roll off factor.

CFO and SCO cause phase rotation, and will distort our data, by the definition of the 802.11n [13], the transmitted center frequency tolerance shall be +/- 20ppm maximum, and the symbol clock frequency tolerance shall be +/- 20ppm maximum. In wireless LANs, four of the sub-carriers are dedicated to pilot signals in order to against frequency offsets and phase noise. The detail algorithms will be described in the chapter 2.

1.3 Organization of this thesis

This thesis is organized as follows: the first chapter briefly introduces 802.11n wireless LAN system and the channel model used for simulation. In chapter 2, the algorithms of CFO mitigation, channel estimation, phase error tracking, and MIMO detection will be described. Simulation results will be analyzed in Chapter 3. The chapter 4 will show the architecture and the techniques of tri-mode hardware implementation. Finally, a brief conclusion and future work will be presented in chapter 5.



Chapter 2

Equalizer Design for WLAN

In this chapter, a tri-mode equalizer design for wireless LAN is proposed. The proposed equalizer includes CFO mitigation, channel estimation, phase error tracking (PET) and MIMO detection. Data distortion caused by multi-path fading, residual CFO and SCO can be eliminated together with equalization.

2.1 System Platform Description

IEEE 802.11n is an OFDM-based indoor WLAN system. We assume there are two transmitted antennas and two received antennas, the block diagrams of the baseband transceiver can be illustrated in Fig 2.1. The transmitted data are coded, MIMO signal processed, interleaved, mapped and modulated by IFFT. Then cyclic prefixes are inserted and OFDM symbols are windowed before upsampling and transmitting through channels.

The MIMO signal processing has two types. SDM is a spatial multiplexing transmission so it can raise the symbol rate to N times by N parallel transmitted antennas. STBC codes the signal at different time and different antennas to achieve transmit diversity. SDM can achieve high speed transmission, and STBC can get excellent system performance on the other hand. These two 2×2 MIMO signal processing are illustrated in Fig 2.2. The techniques of MIMO symbol detection for both MIMO signal will be described in section 2.5.

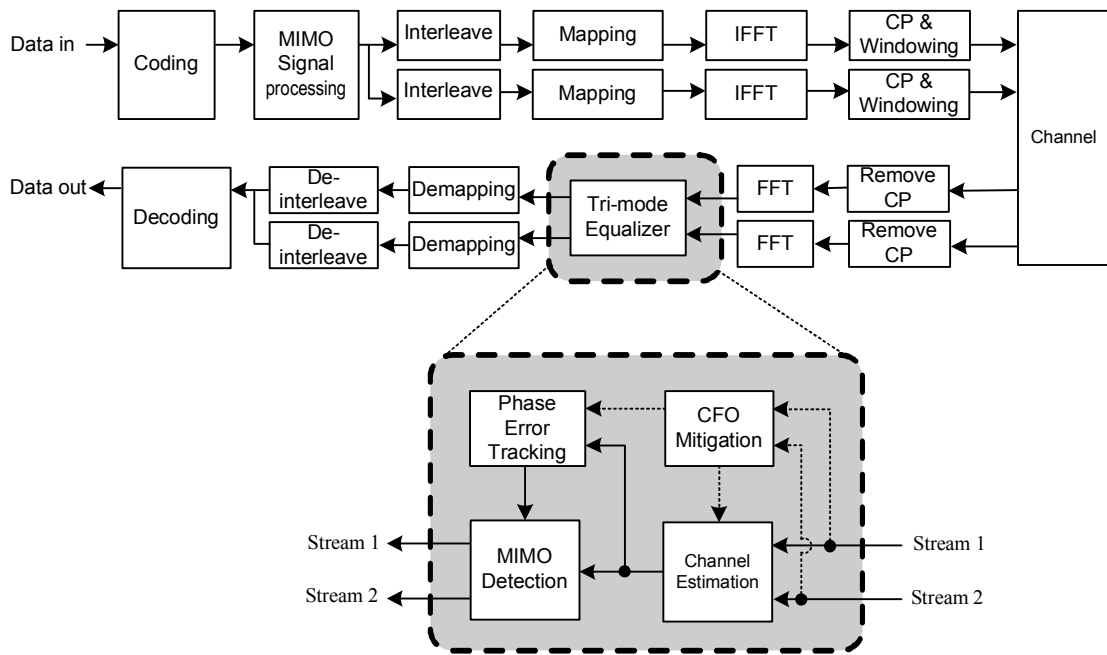


Figure 2.1 System block diagram.

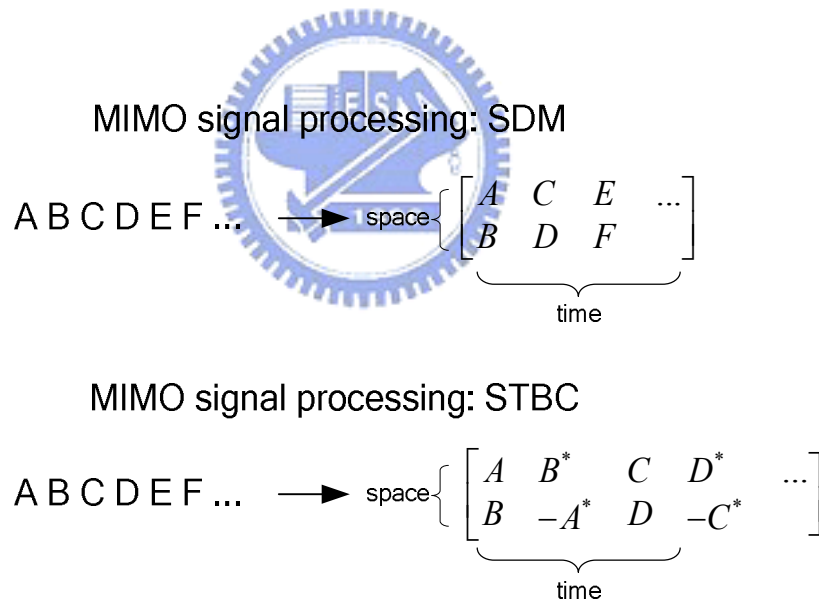


Figure 2.2 2x2 MIMO signal processing.

While receiving, we assume perfect synchronization. Then cyclic prefixes are removed, and signals are transferred to frequency domain by FFT. The following step is equalization. The tri-mode equalizer consists of CFO mitigation, channel estimation, phase error tracking and MIMO detection. The equalizer not only deals

with the channel effect but also compensates the CFO and SCO effects. The algorithms of equalization will be described in detail in the following sections. After equalization, de-mapping, de-interleaving and decoding are processed to recover data.

2.2 CFO Mitigation

To enhance the accuracy of channel estimation, CFO mitigation is utilized to reduce phase errors in the training fields which are used to estimate channels in the mixed-mode of 802.11n.

In 802.11n, the preamble and the header have a Compatibility portion and a High throughput portion for mixed-mode operation [12]. The Compatibility portion of the mixed mode header consists of legacy signal field (L-SIG) can be decoded by non-HT devices, as well as HT devices. What has been observed is that the pilots of the L-SIG, HT-SIG and values in pilot locations in L-LTF in this preamble structure can be utilized for CFO mitigation in HT mixed-mode operation. The training symbols of 802.11n are shown as Fig 2.3.

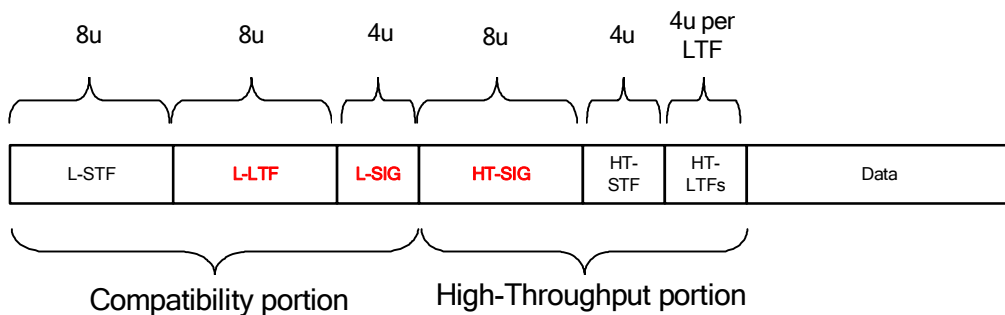


Figure 2.3 Training symbols of 802.11n.

We utilize the concept of the D-symbol estimation [14]. When the remained CFO and SCO are relatively smaller or the Noise is very large, the differences of the rotated phases between two adjacent symbols are very small, as illustrated in Fig.

2.4(a). This may result in poor estimation accuracy and in some cases may give estimation results of the opposite sign. If we compare the phase rotation of the current symbol with the next D symbol that delays D-symbol-interval, demonstrated as Fig. 2.4(b) and (c). the effects of noise may be reduced to some extent. From above conclusions, the proposed CFO mitigation uses 2-symbol estimation to avoid this problem thus gets better performance.

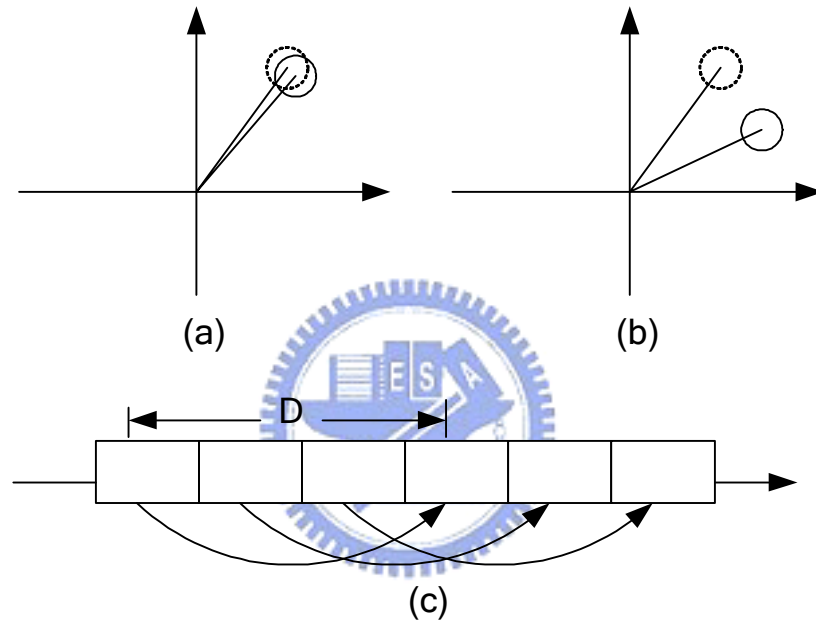


Figure 2.4 The principle of D-symbol estimation [14]

The signal is compensated by CFO and the guard interval is removed before FFT. Under consideration of residual CFO as Δf , SCO as $\delta=(T_s'-T_s)/T_s$, where T_s is the sampling time and T_s' is the offset sampling time. The post-FFT data stream $Y_{l,k,n}$ at the k -th sub-carrier and the n -th receive antenna during l -th OFDM symbol duration can be expressed as:

$$Y_{l,k,n} = e^{j2\pi l\Delta\phi m_l(T_u+T_g)/T_u} \sum_{i_{STS}=1}^{N_{STS}} d_{k,l,i_{STS}} H_{k,i_{STS},n} + w_{k,l,n} \quad (2.1)$$

where $H_{k,i_{sts},n}$ is the frequency response of the channel, T_g is the guard interval, T_u is the duration of FFT, $\Delta\phi \approx \Delta f \cdot T_u + \delta$, m_l is the time-sample index of the first element in the l -th symbol. $d_{k,l,i_{sts}}$ is the complex signal that is transmitted through the k -th sub-carrier and the i_{sts} -th transmitted antenna during l -th OFDM symbol duration. $W_{k,l,n}$ is the noise caused from Additive White Gaussian Noise (AWGN), ICI, phase noise and other non-ideal parameters. Let $\alpha = \Delta f \cdot T_u$ be the phase shift caused from the residual CFO in an OFDM symbol. There (2.1) can be re-written as

$$Y_{l,k,n} = e^{j2\pi l(\delta \cdot k + \alpha)m_l(T_u + T_g)/T_u} \sum_{i_{sts}=1}^{N_{sts}} d_{k,l,i_{sts}} H_{k,i_{sts},n} + w_{k,l,n} \quad (2.2)$$

The received data after FFT at the pilot carrying sub-carriers in the L-LFT, L-SIG and HT-SIG can be rewritten as

$$Y_{l,k,n}^{(p)} = e^{j2\pi l(\delta \cdot k + \alpha)m_l(T_u + T_g)/T_u} \sum_{i_{sts}=1}^{N_{sts}} d_{k,l,i_{sts}}^{(p)} H_{k,i_{sts},n} + w_{k,l,n} \quad (2.3)$$

where $d_{k,l,i_{sts}}^{(p)}$ denotes the transmitted data in the pilot locations. While receiving L-LFT, L-SIG HT-SIG, we can neglect the effects of SCO, i.e., $\Delta\phi \approx \Delta f \cdot T_u$ for convenient because SCO value is relative small compared with CFO at the beginning of a packet. Assume that the channel response is almost static in the duration of a packet which holds true for most indoor scenarios because the duration of a packet is relatively shorter than the coherence time of indoor channel. The pilot patterns in the L-SIG and HT-SIG are defined as the same as pilot patterns in 802.11a standard [15]. The pilot patterns in L-SIG and HT-SIG totally three symbols are exactly identical, so we can directly compute the phase differences between any of the two consecutive symbols. On the other hand, the phase differences between the first L-LTF symbol and L-SIG need to be multiplied by an additional correct vector $\underline{\eta}$. Define the first

received L-LTF symbol as Y_λ . The 2-symbol phase difference $\hat{v}_{i_{sts},1}$ and $\hat{v}_{i_{sts},2}$ can be expressed as:

$$\hat{v}_{i_{sts},1} = \sum_{p=-21,-7,7,21} (Y_{\lambda+2,p,i_{sts}})^* \times Y_{\lambda+4,p,i_{sts}} \quad (2.4)$$

$$\hat{v}_{i_{sts},2} = \sum_{p=-21,-7,7,21} (Y_{\lambda,p,i_{sts}})^* \times Y_{\lambda+2,p,i_{sts}} \times \eta_p \quad (2.5)$$

where $\underline{\eta} = [\eta_7 \ \eta_{21} \ \eta_{-21} \ \eta_{-7}] = [1 \ -1 \ 1 \ -1]$. The training symbols required for proposed CFO mitigation are illustrated as Fig 2.5.

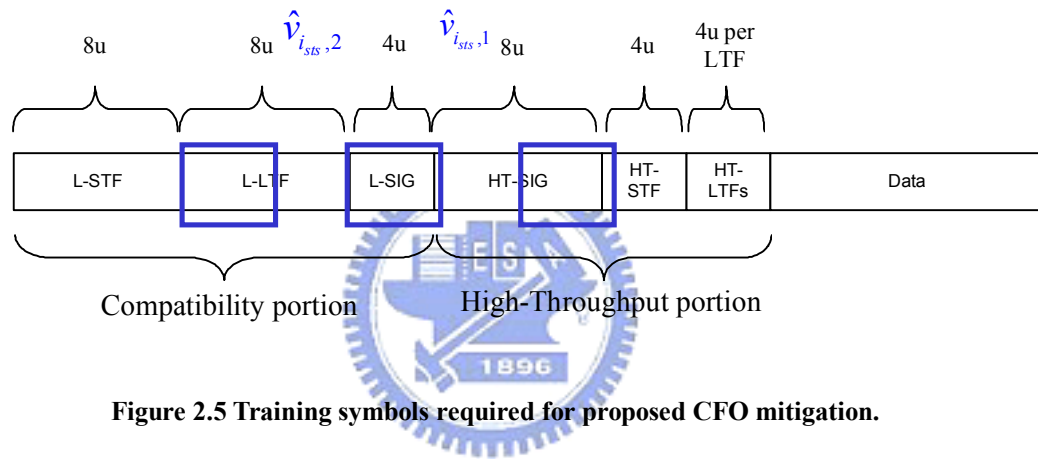


Figure 2.5 Training symbols required for proposed CFO mitigation.

The value of residual CFO is very small after coarse and fine CFO estimation and compensation. To translate the complex-valued signals to phase, arctangent can be approximated by a real divider. The double residual CFO value α' is obtained by averaging over $\hat{v}_{i_{sts},1}$ and $\hat{v}_{i_{sts},2}$. Finally, the residual CFO value $\hat{\alpha}$ can be obtained as:

$$\alpha' = \frac{\sum_k \sum_{i_{sts}} \Im[\hat{v}_{i_{sts},k}]}{\sum_k \sum_{i_{sts}} \Re[\hat{v}_{i_{sts},k}]} \quad (2.6)$$

$$\hat{\alpha} = 0.5 \times \alpha' \quad (2.7)$$

In proposed design, the phase error of HT-LTFs can be compensated by counter rotating the estimated phase in frequency domain with CORDIC modules.

2.3 Channel Estimation

Multipath fading is one of the data distortion issues in OFDM systems. The wideband signal is transmitted over frequency-selective fading channel. The preamble-based channel estimation is generally used under indoor channel because the duration of a packet is relatively shorter than the coherent time, i.e. the channel is assumed to be constant during a packet period. After obtaining the estimated channels, equalization is applied to remove the multipath influence.

(1) SISO mode

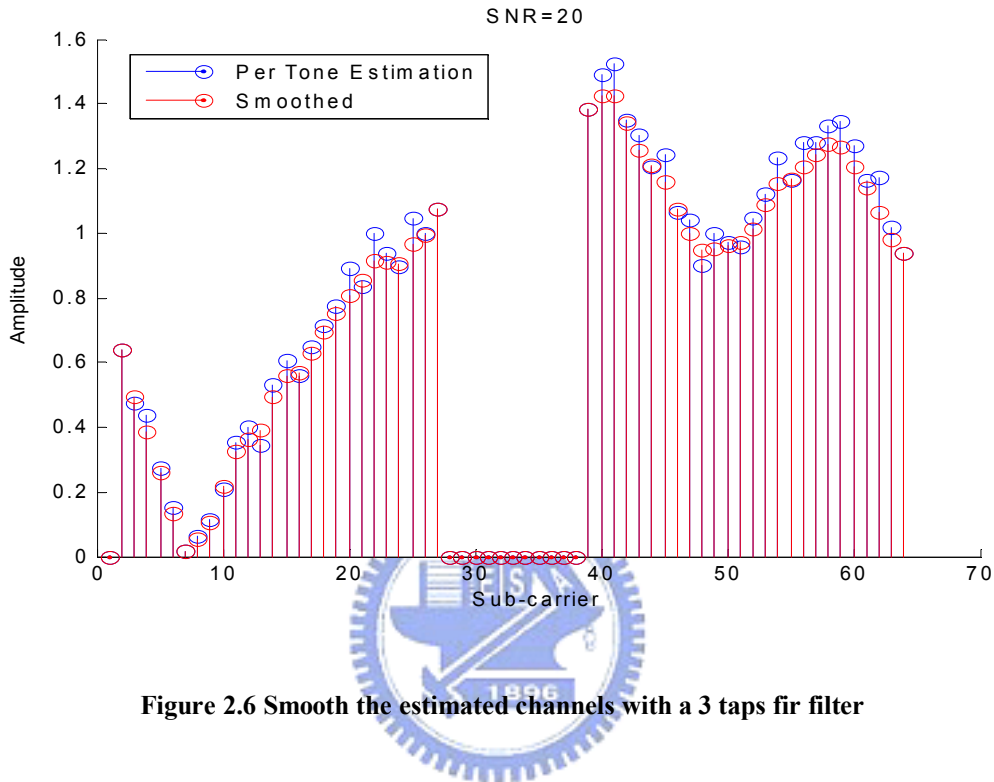
In OFDM-based wireless LAN systems, preamble-based Zero Forcing channel estimation is generally applied to estimate the channel frequency response for SISO mode due to its advantage of low complexity. The pre-known signal is defined as $a_{l,k}$ in the preamble with $l = \lambda, \lambda + 1$. Using the feature of the repeated structure in of long preamble in frequency domain, we can average the result of twice Zero Forcing estimations to suppress noise. The estimate of k -th sub-channel is generally given by

$$\hat{H}_k = \frac{1}{2} \left(\frac{Y_{\lambda,k}}{a_{\lambda,k}} + \frac{Y_{\lambda+1,k}}{a_{\lambda+1,k}} \right) \quad (2.8)$$

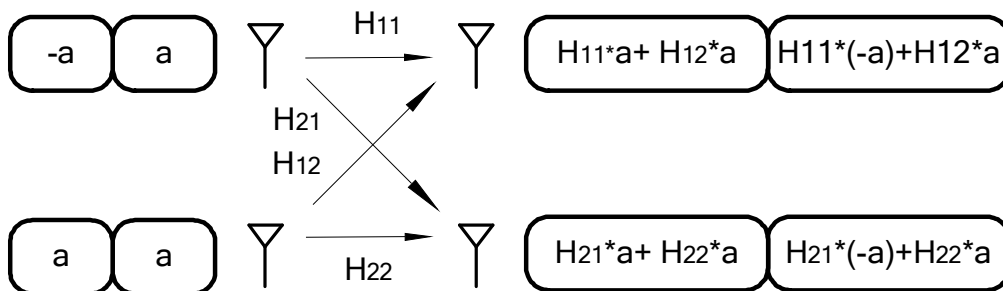
The pre-known signal $a_{l,k}$ is 1 or -1 so the dividers can be avoided. Thus Equation 2.8 can be modified as

$$\hat{H}_k = 0.5 \times a_{\lambda,k} \times (Y_{\lambda,k} + Y_{\lambda+1,k}) \quad (2.9)$$

The estimated channels can be improved further by passing them through a smooth filter. We use a three taps $[0.25 \ 0.5 \ 0.25]$ FIR filter based on the correlative property between adjacent sub-carriers. The smoothed channels are compared with the results of the per tone estimation only in Fig 2.6.



(2) 2x2 MIMO modes (SDM-MIMO/ STBC-MIMO)



For 2x2 MIMO transmissions for 802.11n, there are two symbol durations for HT-LTF. The relationship between the transmitted preambles and the combinations of

the signals in receiver are illustrated as Fig. 2.7. We note that the HT-LTF is transmitted in Alamouti form for 2x2 MIMO. The pre-known signal is defined as a_k in the preamble, and the received preamble signals of k -th sub-channel can be expressed as:

$$\begin{pmatrix} Y_{r1,\lambda+6,k} \\ Y_{r2,\lambda+6,k} \end{pmatrix} = \begin{pmatrix} H_{11,k} & H_{12,k} \\ H_{21,k} & H_{22,k} \end{pmatrix} \begin{pmatrix} a_k \\ a_k \end{pmatrix} + N_{2 \times 1} \quad (2.10)$$

$$\begin{pmatrix} Y_{r1,\lambda+7,k} \\ Y_{r2,\lambda+7,k} \end{pmatrix} = \begin{pmatrix} H_{11,k} & H_{12,k} \\ H_{21,k} & H_{22,k} \end{pmatrix} \begin{pmatrix} -a_k \\ a_k \end{pmatrix} + N_{2 \times 1} \quad (2.11)$$

where $Y_{r1,l,k}$ and $Y_{r2,l,k}$ are the received signals of l -th symbol and k -th sub-channel at receiving stream 1 and stream 2 respectively. We can observe that all channel frequency responses can be obtained by simple linear combinations.

After linear combination, the 2x2 MIMO channel estimates of k -th sub-channel are given by:

$$\hat{H}_{2 \times 2,k} = 0.5 \times \frac{1}{a_k} \times \begin{pmatrix} Y_{r1,\lambda+6,k} - Y_{r1,\lambda+7,k} & Y_{r1,\lambda+6,k} + Y_{r1,\lambda+7,k} \\ Y_{r2,\lambda+6,k} - Y_{r2,\lambda+7,k} & Y_{r2,\lambda+6,k} + Y_{r2,\lambda+7,k} \end{pmatrix} \quad (2.12)$$

The pre-known signal a_k is 1 or -1 so complex dividers can be avoided. Thus equation 2.12 can be modified as

$$\hat{H}_{2 \times 2,k} = 0.5 \times a_k \times \begin{pmatrix} Y_{r1,\lambda+6,k} - Y_{r1,\lambda+7,k} & Y_{r1,\lambda+6,k} + Y_{r1,\lambda+7,k} \\ Y_{r2,\lambda+6,k} - Y_{r2,\lambda+7,k} & Y_{r2,\lambda+6,k} + Y_{r2,\lambda+7,k} \end{pmatrix} \quad (2.13)$$

2.4 Phase Error Tracking

Carrier Frequency offset (CFO) and sampling clock offset (SCO) are the other two major data distortion issues in OFDM systems. Though CFO has been mitigated by coarse and fine CFO estimation in time domain, the CFO error (or residual CFO)

in data portion still can not be neglected. Residual CFO and SCO rotating the received data in constellation diagrams cause great data errors while receiving. Phase error tracking (PET) is generally applied to trace the phase rotation caused by residual CFO and SCO; Fig. 2.8 shows the 64QAM constellation with and without PET.

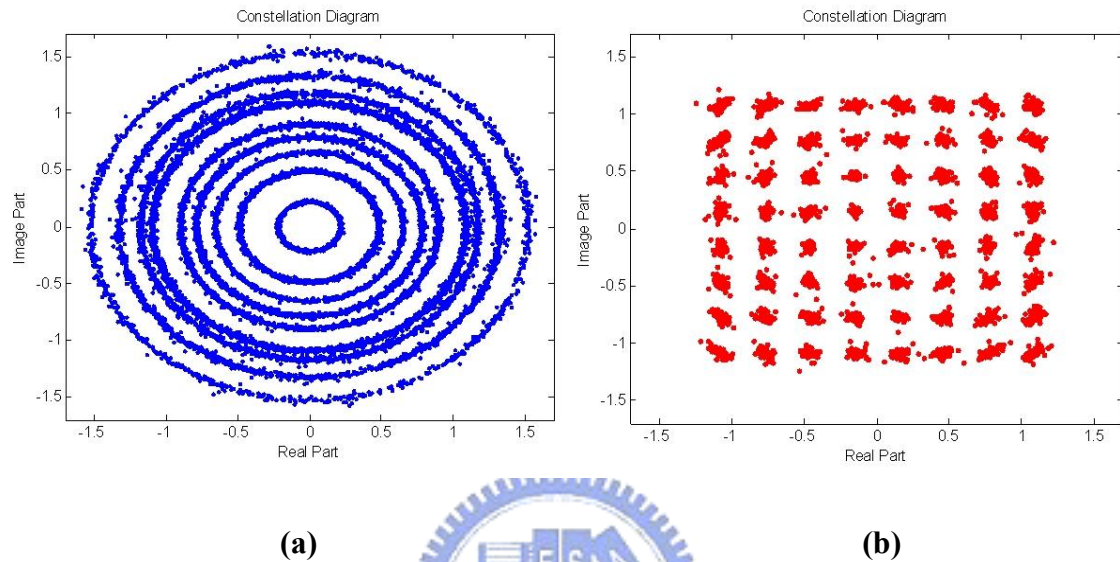


Figure 2.8 64QAM data constellation: (a) without PET (b) with PET

2.4.1 Carrier Frequency Offset Tracking

In this section, an Least Mean Square (LMS) based adaptive CFO tracker is proposed. Considering the integration of the three modes, different but similar algorithms are used here in order to get a good trade-off between performance and computational complexity. The proposed CFO tracking has three steps to complete the adaptive recursion.

Step 1. Pilot Pre-compensation

When the packet length is long, the phase error caused by residual CFO may exceed the $\pm\pi$ range. This will cause large estimation error while tracking residual CFO using conventional PET. The pilot pre-compensation concept [16] is utilized to solve this problem. The received data after pilot pre-compensation is written as:

$$Y'_{\lambda+m,i_{STS},k} = Y_{\lambda+m,i_{STS},k} \cdot e^{-j\hat{\phi}_{\lambda+m-1,k}} \quad (2.14)$$

$$i_{STS} = 1, 2; \quad k = -21, -7, 7, 21$$

where $\hat{\phi}_{\lambda+m-1}$ is the phase error at $(\lambda+m-1)$ -th symbol.

Step 2. Phase Estimation

After pilot pre-compensation, the detected pilot phase is the difference between two adjacent OFDM symbols. The detected pilot phases in complex form can be written as:

$$\hat{u}_{\lambda+m,i_{STS},k} = Y'_{\lambda+m,i_{STS},k} \cdot \text{conj} \left(\sum_{i_{TX}=1}^{N_{TX}} P_{\lambda+m,i_{STS},k} \hat{H}_{i_{STS},i_{TX},k} \right) \quad (2.15)$$

$$i_{STS} = 1, 2; \quad k = -21, -7, 7, 21$$

where $P_{\lambda+m,i_{STS},k}$ is the transmitted pilot value of k -th sub-carrier of i_{STS} -th transmitted antenna during $(\lambda+m)$ -th OFDM symbol duration. The pilots occupies at $k = -21, -7, 7, 21$ in each OFDM symbol.

To average the phases over receiving streams and pilot sub-carriers, We use two different methods to obtain mean phase error in the three modes. Linear Least Square (LLS) [14] is utilized in SDM-MIMO and STBC-MIMO modes, and Weighted Least Square (WLS) [17] is utilized in SISO mode on the other hand. LLS has the advantage of low computational complexity, but has bad performance in the condition of few pilot numbers, especially in low SNR conditions. WLS has better performance than LLS by using the information of signal's power but pays the price of more complexity in hardware. In the 2x2 SDM-MIMO and STBC-MIMO modes, there are eight pilots from two data streams totally, but there are only four pilots for PET utilization in SISO mode. For these reasons, we use WLS and LLS to estimate the phase rotations from residual CFO in SISO mode and SDM-MIMO/STBC-MIMO

modes, respectively.

Linear Least Square for SDM-MIMO/STBC-MIMO modes:

$$\hat{u}_{\lambda+m} = \sum_{i_{sts}} \sum_{k=-21,-7,7,21} \hat{u}_{\lambda+m,i_{sts},k} \quad (2.16)$$

$$\alpha'_{\lambda+m} = \frac{\Im[\hat{u}_{\lambda+m}]}{\Re[\hat{u}_{\lambda+m}]} \quad (2.17)$$

Weighted Least Square for SISO mode:

$$w_{\lambda+m,k} = |Y_{\lambda+m,k}|^2 \quad (2.18)$$

$$\tilde{\alpha}_{\lambda+m,k} = \frac{\Im[\hat{u}_{\lambda+m,i_{sts},k}]}{\Re[\hat{u}_{\lambda+m,i_{sts},k}]} \quad (2.19)$$

$$\alpha'_{\lambda+m} = \frac{\sum_{k=-21,-7,7,21} w_{\lambda+m,k} \tilde{\alpha}_{\lambda+m,k}}{\sum_{k=-21,-7,7,21} w_{\lambda+m,k}} \quad (2.20)$$

where $w_{\lambda+m,k}$ is the weighted coefficients of k -th sub-carrier during $(\lambda+m)$ -th OFDM symbol duration and it is calculated from the power of received data, $\alpha'_{\lambda+m}$ is the estimated phase shift from residual CFO between $(\lambda+m-1)$ -th and $(\lambda+m)$ -th symbols. To get the pilot phase difference between two adjacent symbols from complex value \hat{u} , the arctangent operation can be approximated by a real divider because the phase difference values are very small between two adjacent symbols.

Step 3. Recursive Adjustment

In step 3, we calculate the error vector to update the residual CFO value in current symbol.

$$\Theta_{\lambda+m} = \alpha'_{\lambda+m} - \hat{\alpha}_{\lambda+m-1} \quad (2.21)$$

$$\hat{\alpha}_{\lambda+m} = \hat{\alpha}_{\lambda+m-1} + \mu_0 \Theta_{\lambda+m} \quad (2.22)$$

$$\hat{\phi}_{\lambda+m} = (\hat{\delta}_{\lambda+m} \cdot k + \hat{\alpha}_{\lambda+m}) \cdot (\lambda + m) \quad (2.23)$$

$$m = \begin{cases} 2, 3, 4 \dots & , \text{ SISO mode} \\ 8, 9, 10 \dots & , \text{ SDM-MIMO/STBC-MIMO modes} \end{cases}$$

where u_0 is the step size which is chosen to the power of two for implementation consideration. $\Theta_{\lambda+m}$ is the error vector at $(\lambda+m)$ -th symbol, $\hat{\alpha}_{\lambda+m}$ is the new updated phase shift caused by residual CFO at $(\lambda+m)$ -th symbol, $\hat{\delta}_{\lambda+m}$ is the estimated phase shift caused by SCO at $(\lambda+m)$ -th symbol and $\hat{\phi}_{\lambda+m}$ is the estimated phase error at $(\lambda+m)$ -th symbol. The method to obtain $\hat{\delta}_{\lambda+m}$ is described at next section.

The first estimate of residual CFO for SISO mode can be obtained by

$$\hat{\alpha}_{\lambda+1} = \frac{\sum_k (\hat{\phi}_{\lambda+1,k} - \hat{\phi}_{\lambda,k})}{52} \quad (2.24)$$

The first estimate of residual CFO for SDM-MIMO/STBC-MIMO modes can be obtained from in (2.7):

$$\hat{\alpha}_{\lambda+7} = \hat{\alpha} \quad (2.25)$$

2.4.2 Sampling Clock Offset Tracking

Assume that carrier frequency and sampling time are generated by the same reference oscillator in receiver as suggestion of 802.11n specification [13]. The phase shifts caused from CFO ε and SCO δ have the following relationship:

$$\varepsilon = (f_c \cdot T_{FFT}) \cdot \delta \quad (2.26)$$

where f_c is carrier frequency and T_{FFT} is the duration of FFT.

2.5 MIMO Detection

In this section, one tap channel equalizer for SISO mode and two types of 2x2 MIMO symbol detectors for SDM-MIMO and STBC-MIMO are introduced respectively. The complexity in hardware is important considering implementation. Zero Forcing (ZF) having low complexity is generally used in SISO mode for wireless LAN. The optimal SDM-MIMO symbol detector is the maximal likelihood (ML) detector, but its complexity increases exponentially with number of transmit antennas and modulation order [18]. Sphere decoding scheme has the main disadvantage of lots delay. Vertical Bell Labs Layered Space-Time (V-BLAST) is a sub-optimal solution also requires lots of computational complexity on ordered-successive-interference cancellation (OSIC). On the other hand, minimal mean square error (MMSE) provides a good trade-off between performance and complexity for SDM-MIMO detection. The data encoded by STBC has an advantage of low complexity in receiver. The data is transmitted in Alamouti form for 2x2 STBC-MIMO mode, so maximal likelihood (ML) symbol detection can be utilized to decode STBC-MIMO signals.

2.5.1 Zero Forcing channel equalizer for SISO mode

The ZF channel equalizer can be expressed as

$$\hat{X}(k) = \frac{Y(k)}{\hat{H}_k} \quad (2.27)$$

where \hat{X}_k is the equalized signal of k-th subcarrier. In Equation (2.27), received data Y_k is divided by the estimated Channel Frequency Response to eliminate multipath fading.

2.5.2 Minimal Mean Square Error SDM-MIMO Symbol Detection

The channel matrix coefficients of the k -th subcarrier are given by:

$$H_k = \begin{pmatrix} h_{1,k} & h_{3,k} \\ h_{2,k} & h_{4,k} \end{pmatrix} \quad (2.28)$$

It operates under the same subcarrier in the following, so we let $h_{m,k}=h_m$, $H_k=H$.

Equation (2.28) can be re-written as:

$$H = \begin{pmatrix} h_1 & h_3 \\ h_2 & h_4 \end{pmatrix} \quad (2.29)$$

The receiving signals can be modeled as:

$$Y(k)=H \cdot X(k)+N(k) \quad (2.30)$$

where $Y(k)$ and $X(k)$ are the received and transmitted signals of k -th subcarrier respectively, and $N(k)$ is the noise term.

We define an error vector $e(k)$ which is the difference between the transmitted signals and the received signals which have passed through MMSE filter. $e(k)$ is defined as :

$$e(k)=X(k)-G^H Y(k) \quad (2.31)$$

where G is the MMSE filter. We define the cost function J as:

$$J=E \{e^H(k)e(k)\} \quad (2.32)$$

Because J is a scalar value, it can be re-written as:

$$J=\text{tr}[E \{e(k)e^H(k)\}] \quad (2.33)$$

To minimize cost function J , we set zeros to the complex gradient vector ∇J , then

Wiener-Hopf equation is obtain as:

$$G^H R_{YY} = R_{XY} \quad (2.34)$$

where

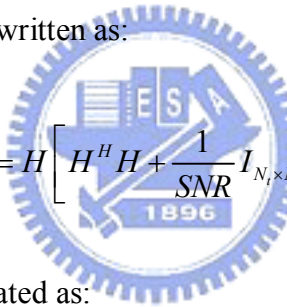
$$R_{YY} = E\{Y(k)Y(k)^H\} \quad R_{XY} = E\{X(k)Y(k)^H\} \quad (2.35)$$

where R_{YY} is the covariance of the received signals and R_{XY} is the cross-correlation of the transmitted and received signals.

From Equation (2.34), we can obtain MMSE filter as:

$$G = \left[HH^H + \frac{1}{SNR} I_{N_r \times N_r} \right]^{-1} H \quad (2.36)$$

and Equation (2.36) can be re-written as:

$$G = H \left[H^H H + \frac{1}{SNR} I_{N_r \times N_r} \right]^{-1} \quad (2.37)$$


The noise power can be calculated as:

$$\frac{1}{N} \sum_{k=0}^{N-1} |Y_{p1}(k) - Y_{p2}(k)|^2 = \frac{1}{N} \sum_{k=0}^{N-1} |\Delta N_1(k) - \Delta N_2(k)|^2 \approx 2\sigma^2 \quad (2.38)$$

$$\hat{\sigma}^2 = \frac{1}{2N} \sum_{k=0}^{N-1} |Y_{p1}(k) - Y_{p2}(k)|^2 \quad (2.39)$$

Finally, we can obtain the decoding signal as:

$$\hat{X}(k) = G^H \cdot Y(k) \quad (2.40)$$

The constellations after MMSE detection are shown as Fig. 2.9.

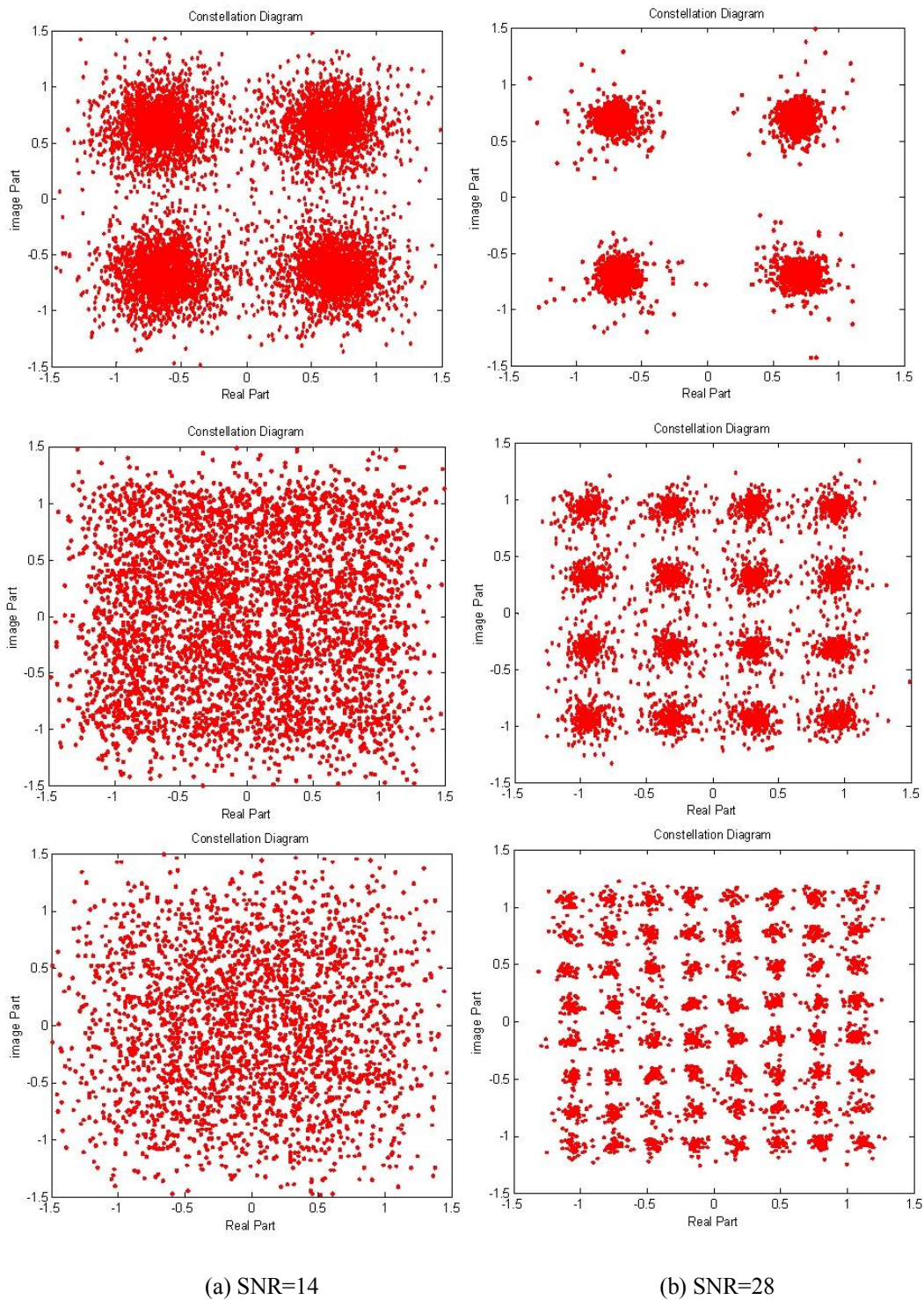


Figure 2.9 Constellation diagram of MMSE detection under different SNR.

2.5.2 Maximal Likelihood STBC-MIMO Symbol Detection

Example of the 2x2 STBC-MIMO transmissions:

Table 2.1 Transmitted signals for 2x2 STBC-MIMO

	TX1	TX2
Symbol 1	S_0	S_1
Symbol 2	$-S_1^*$	S_0^*

The receiving signal for 2x2 STBC-MIMO can be express as:

$$\begin{pmatrix} y_0^0 \\ y_0^1 \end{pmatrix} = \overbrace{\begin{pmatrix} s_0 & s_1 \\ -s_1^* & s_0^* \end{pmatrix}}^{tx} \begin{pmatrix} h_1 \\ h_3 \end{pmatrix} + \begin{pmatrix} n_0^0 \\ n_0^1 \end{pmatrix} \quad (2.41)$$

$$\begin{pmatrix} y_1^0 \\ y_1^1 \end{pmatrix} = \overbrace{\begin{pmatrix} s_0 & s_1 \\ -s_1^* & s_0^* \end{pmatrix}}^{tx} \begin{pmatrix} h_2 \\ h_4 \end{pmatrix} + \begin{pmatrix} n_1^0 \\ n_1^1 \end{pmatrix} \quad (2.42)$$

where y_i^j represents the receiving signal of i -th receiving antenna at j -th symbol.

Equations (2.41) and (2.42) can be transferred as:

$$\begin{pmatrix} y_0^0 \\ y_0^{1*} \end{pmatrix} = \overbrace{\begin{pmatrix} h_1 & h_3 \\ h_3^* & -h_1^* \end{pmatrix}}^{tx} \begin{pmatrix} s_0 \\ s_1 \end{pmatrix} + \begin{pmatrix} n_0^0 \\ n_0^{1*} \end{pmatrix} \quad (2.43)$$

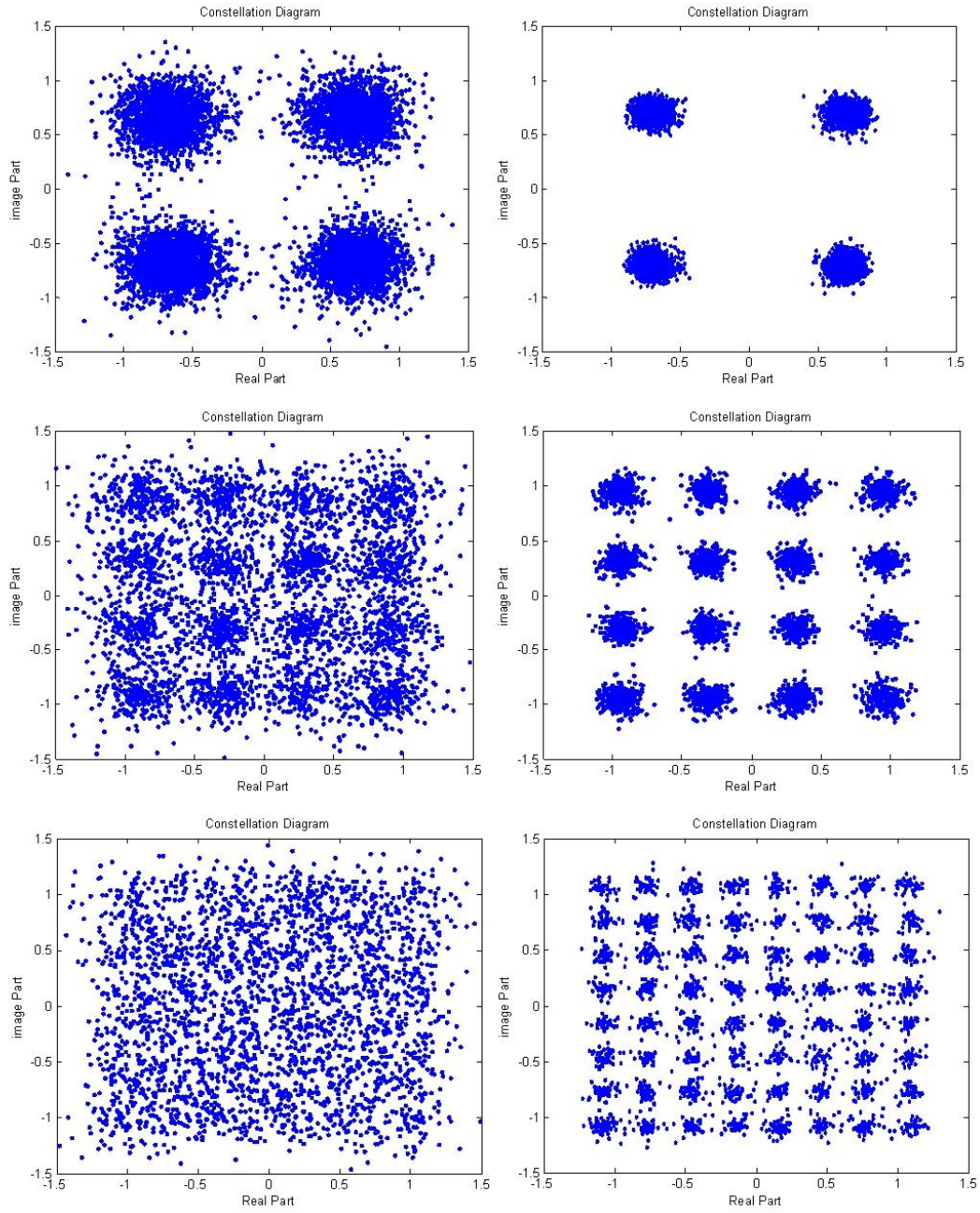
$$\begin{pmatrix} y_1^0 \\ y_1^{1*} \end{pmatrix} = \overbrace{\begin{pmatrix} h_2 & h_4 \\ h_4^* & -h_2^* \end{pmatrix}}^{tx} \begin{pmatrix} s_0 \\ s_1 \end{pmatrix} + \begin{pmatrix} n_1^0 \\ n_1^{1*} \end{pmatrix} \quad (2.44)$$

Then Equations (2.43) and (2.44) are multiplied by the Hermitian transpose of the channel gain matrix, respectively:

$$(|h_1|^2 + |h_2|^2 + |h_3|^2 + |h_4|^2) \begin{pmatrix} s_0 \\ s_1 \end{pmatrix} = \begin{pmatrix} h_1^* & h_3 \\ h_3^* & -h_1 \end{pmatrix} \begin{pmatrix} y_0^0 \\ y_0^{1*} \end{pmatrix} + \begin{pmatrix} h_2^* & h_4 \\ h_4^* & -h_2 \end{pmatrix} \begin{pmatrix} y_1^0 \\ y_1^{1*} \end{pmatrix} + N \quad (2.45)$$

where N is the linear combination of noise. We can obtain the estimated signal by dividing $|h_1|^2 + |h_2|^2 + |h_3|^2 + |h_4|^2$. The constellations after ML detection are shown as

Fig. 2.10.



(a) SNR=10

(b) SNR=18

Figure 2.10 Constellation diagram of ML detection under different SNR.

Chapter 3

System Simulation and Performance Analysis

In this chapter, we will discuss the design flow, system platform and performance for the proposed design. A complete baseband system platform on MATLAB is established compliant to 802.11n draft to verify the proposed design. Channel estimation accuracy, PET performance and PER for overall system will be simulated and be compared with conventional approaches.

3.1 Design and Verification Flow

In design and verification flow as shown in Fig 3.1, we first have to understand the design requirements. Second, appropriate algorithms can be determined for proposed design, and then be simulated in float point on MATLAB to evaluate whether it meets the specification requirements. Next, word length in each operation will be determined to compromise between performance and complexity in fixed point simulation. The simulation on MATLAB is completed here if the performance of fixed point simulation meets specification requirements. The RTL code is developed according to the fixed point simulation and then is synthesized by XST Synthesizer built in Xilinx ISE. Finally the flow is completed after FPGA verification.

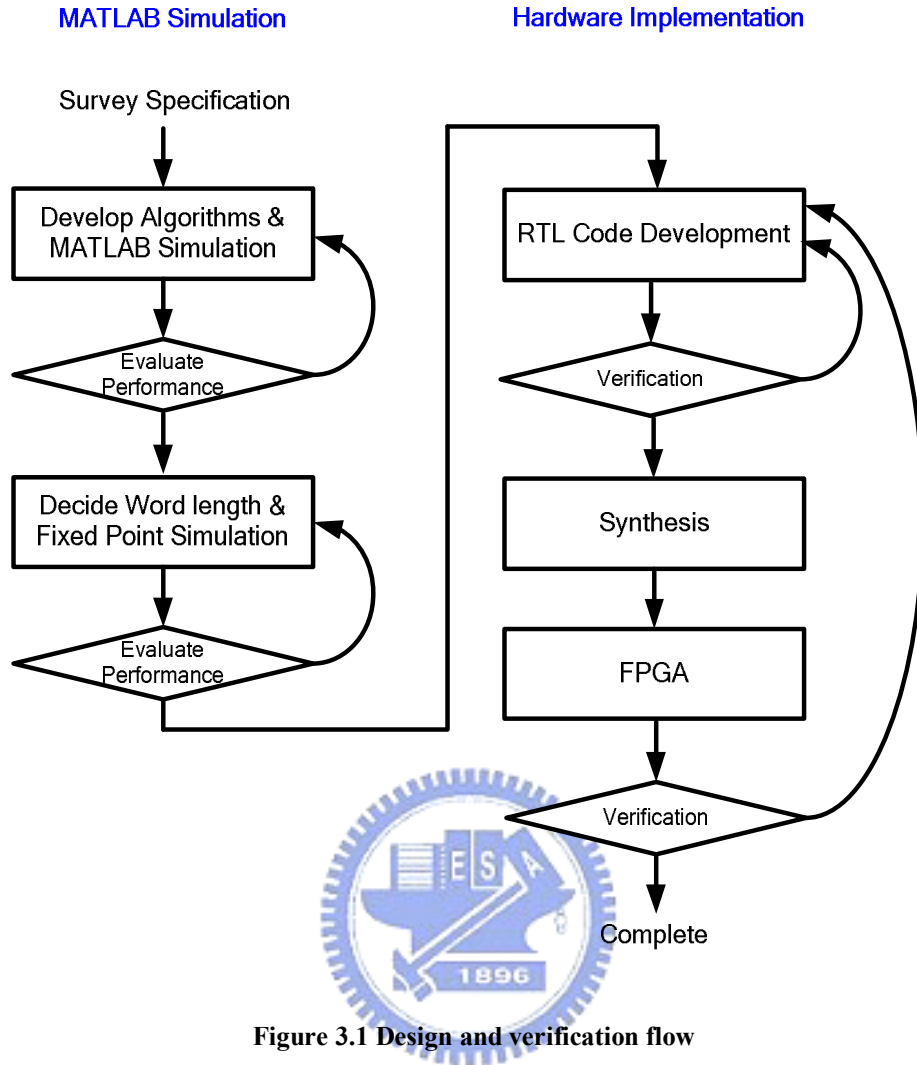


Figure 3.1 Design and verification flow

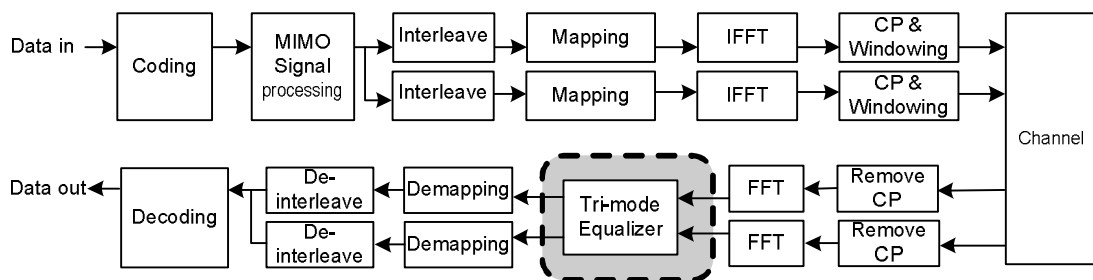


Figure 3.2 The system platform on MATLAB

3.2 System Platform on MATLAB

Our system platform on MATLAB is illustrated as Fig 3.2. The platform is built based on IEEE 802.11n draft and the simulated channel has been introduced in

chapter 1. The parameters of the system environment are set according to IEEE 802.11 TGn Comparison Criteria 67 [6]:

- Trace-back length of Viterbi decoder is 128.
- No smoothing filter for channel estimation, i.e., per tone estimation
- PPDU length is 1000 bytes.
- SNR is calculated as ensemble averaged SNR.
- When the number of packet error reaches to 100, then quit from this loop.
- 20,000 seeds of channel realization are used

Physical layer impairments added in our platform include

- IM2 (Carrier frequency offset)
Offset value is -20ppm, and sampling clock offset is also added.
- IM6 (Antenna Configuration)
Antenna configuration is linear array and distance between adjacent two antennas is a half wavelength.

In our simulations, we have one FEC encoder and two spatial streams. Rate 1/2 convolutional coding is employed. Also, 800 ns Guard interval is used. The IEEE indoor MIMO WLAN channel model 'D' [5] in the condition of non line of sight (NLOS) is applied. No beamforming is considering in our system.

3.3 Performance Analysis

The performance of the tri-mode equalizer for 802.11n will be simulated and analyzed in this section. We will focus on the 10% PER in system performance, which is the requirement of IEEE 802.11n standard.

3.3.1 Channel Estimation Accuracy Analysis

Channel estimation accuracy is highly related to the effects of residual CFO in preamble portion for 802.11n as introduced in chapter 2. HT-LTFs are used to estimate MIMO channels in preamble based channel estimation, and the residual CFO in HT-LTFs can be suppressed by CFO mitigation. So channel estimation accuracy is used to analyze the performance of CFO mitigation. We first define the mean channel estimation error as

$$\text{Mean} \left\{ \sum_{i=1}^M \sum_{j=1}^N |H_{i,j,k} - \hat{H}_{i,j,k}| / (MN) \right\} \quad (3.1)$$

where $\hat{H}_{i,j,k}$ is the ij -th element of estimated channel frequency response of k -th subcarrier and $M \times N$ is the dimension of H_k . Fig. 3.3 shows the residual CFO effects on channel estimation error under different CFO mitigation algorithms for 802.11n (2x2 system) on a TGn D channel.

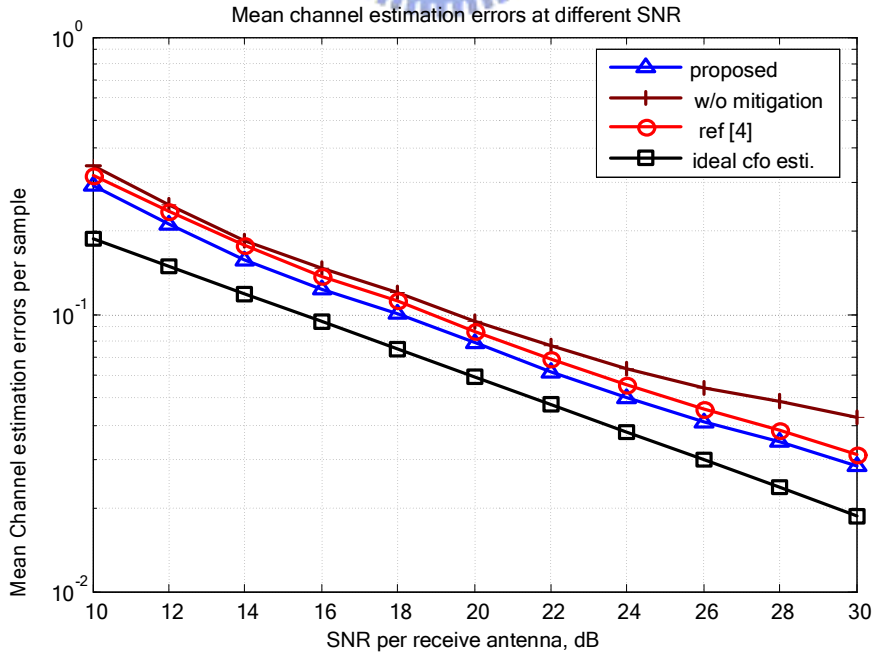


Figure 3.3 Mean channel estimation errors vs. SNR under different CFO mitigation algorithms.

The proposed CFO mitigation achieves 1.0~4.0dB SNR gain in mean channel error compared with conventional one which is without CFO mitigation. Compared with the method used in [4], there are still 0.5~2.0dB SNR improvement in mean channel error, so the proposed CFO mitigation algorithm increases the accuracy of channel estimation effectively.

3.3.2 Phase Error Tracking Performance Analysis

CFO is one of the main factors to degrade system Packet Error Rate (PER) performance. In order to verify the PET performance, the design is simulated under 40ppm CFO, which is standard requirement. The transmission is under QPSK and 1/2 coding rate. Fig 3.4 shows that different PET algorithms are compared for 802.11n (2x2 system) on PER performance. We notice that conventional weighted average method [14] can not get good performance and mean average method [16] is even worse. As mentioned in chapter 1, the pilot-based PET can not suppress noise enough to get a satisfied PER performance due to few pilot numbers in WLAN systems,

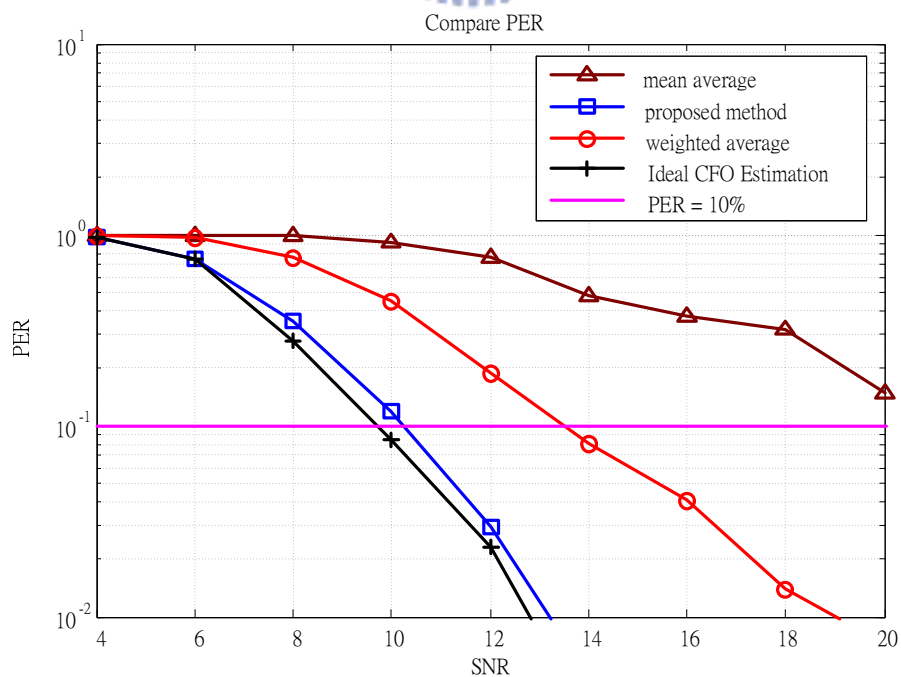


Figure 3.4 Compare PET Algorithms at 2x2 MIMO, QPSK, 1/2 Code rate.

especially in low SNR region. There are only 4 pilots can be utilized per data symbol in one data stream for wireless LAN systems. On the other hand, the proposed adaptive CFO tracking algorithm suppresses the PER loss due to residual CFO within 0.2 dB for 802.11n (2x2 system) compared with ideal CFO estimation. From Fig. 3.4, the proposed adaptive PET achieves 3.0 dB gains than weighted average one at 10% PER requirement. We can conclude the proposed PET increases the system performance a lot.

3.3.3 System Performance

To verify the complete system performance of the proposed tri-mode channel equalizer, PER of a complete IEEE 802.11n basdband processor are simulated with the TGn proposed indoor wireless channel model D and non-ideal impairments of 40ppm CFO and 40ppm SCO in receiver.

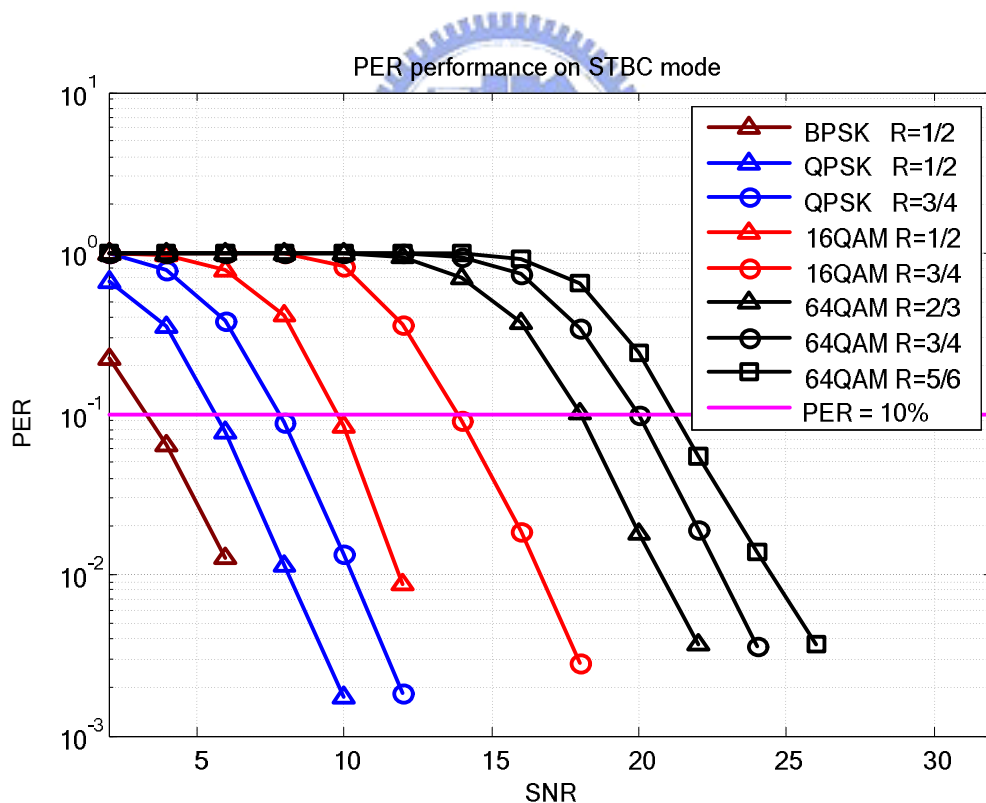
The required SNR for SISO and SDM-MIMO modes to achieve 10% PER are listed in Table 3.1. The proposed baseband system can achieve 0.2~3.8dB and 0.2~1.2dB SNR gain compared with TGn proposed results [19] and [20], respectively.

Table 3.1 PER Performance Comparison on SISO/SDM

MCS	4	9	12	15
Modulation	16 QAM	4 QAM	16 QAM	64 QAM
MIMO	1x1	2x2	2x2	2x2
Coding Rate	$\frac{3}{4}$	$\frac{1}{2}$	$\frac{3}{4}$	$\frac{5}{6}$
Data Rate(Mbps)	39	26	78	130
Required SNR, TGn [1]	N/A	14	26.5	35.5
Required SNR, PLL Based [2]	23	N/A	25	33.5
Required SNR, This Work	21.8	10.2	24.5	33.3
Required SNR, Ideal	21	10	24.4	33.3

Higher performance can be obtained in the proposed baseband receiver because the effects of CFO are outstandingly suppressed by the proposed CFO mitigation and adaptive PET.

The PER curves of different transmission modes for STBC-MIMO (2x2 system) are shown in Fig. 3.5. System constraint for 802.11a and the required SNR to meet 10% PER for STBC-MIMO for 802.11n are listed in Table 3.2. We note that much better performance can be obtained compared with legacy SISO systems due to space diversity of an additional antenna. Especially in low SNR region, outstanding performance can be achieved, thus suitable for low data rate and high performance transmission.



**Figure 3.5 PER performance on STBC mode under TGn channel model D,
40ppm CFO and 40 ppm SCO**

**Table 3.2 System constraint for 802.11a and the required SNR to meet 10% PER
for STBC-MIMO for 802.11n**

802.11a		STBC-MIMO for 802.11n	
Data Rate	System Constraint (dB)	Data Rate	Required SNR (dB)
6	9.7	6.5	3
9	10.7	13	6
12	12.7	19.5	8
18	14.7	26	10
24	17.7	39	14
36	21.7	52	18
48	25.7	58.5	20
54	26.7	65	21



Chapter 4

Hardware Implementation

In chapter 2, we proposed a tri-mode equalizer for OFDM-based wireless LAN. Considering hardware implementation efficiently for tri-mode equalizer design, many shared-architectures based on common algorithms and different working timing are derived and utilized in this chapter.

4.1 Common Architecture Design for Tri-mode Equalizer

We proposed a common architecture design for tri-mode equalizer as shown in Fig. 4.1. We note that a Coordinate Rotation Digital Computer (CORDIC) is used to compensate phase errors in our equalizer design. CORDIC is a well-known iterative method for the computation of vector rotation. Compared to Look-up-tables (LUTs), CORDIC reduces the complexity by using adders, shifters, and comparators.

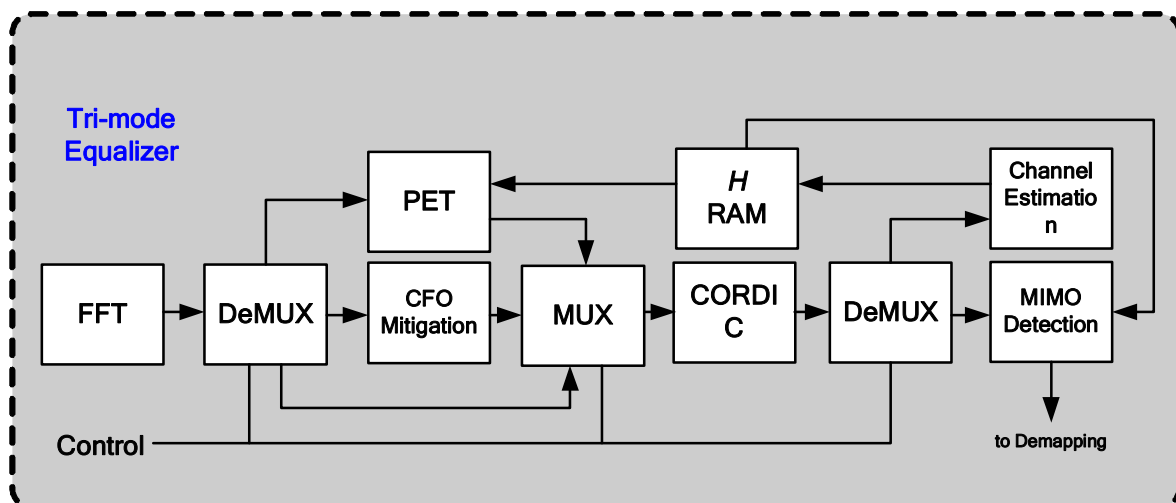


Figure 4.1 Tri-mode equalizer architecture

The signals after FFT will go in CFO mitigation first for SDM-MIMO and STBC-MIMO modes or will bypass it for SISO mode, and then the estimated residual CFO in HT-LTFs will be compensated by CORDIC. The High-Throughput Long Training Fields (HT-LTFs) are used to estimate MIMO channels for SDM-MIMO/STBC-MIMO modes and Legacy Long Training Field (LLF) is used to estimate channel for SISO mode. The estimated channels then will be saved in RAMs. With estimated channels, PET can track the phase errors caused by residual CFO and SCO. Then send to CORDIC in the same manner to compensate phase errors in data portion. Here we notice that one CORDIC can be fully utilized for two times because CFO mitigation and PET work at different timings. Finally, the data after CORDIC will be equalized by MIMO detection. In the following section, the modules in tri-mode equalizer will be described in detail.



4.2 Modules Design

4.2.1 CFO Mitigation Module Design

The proposed architecture of CFO mitigation is shown as Fig. 4.2.

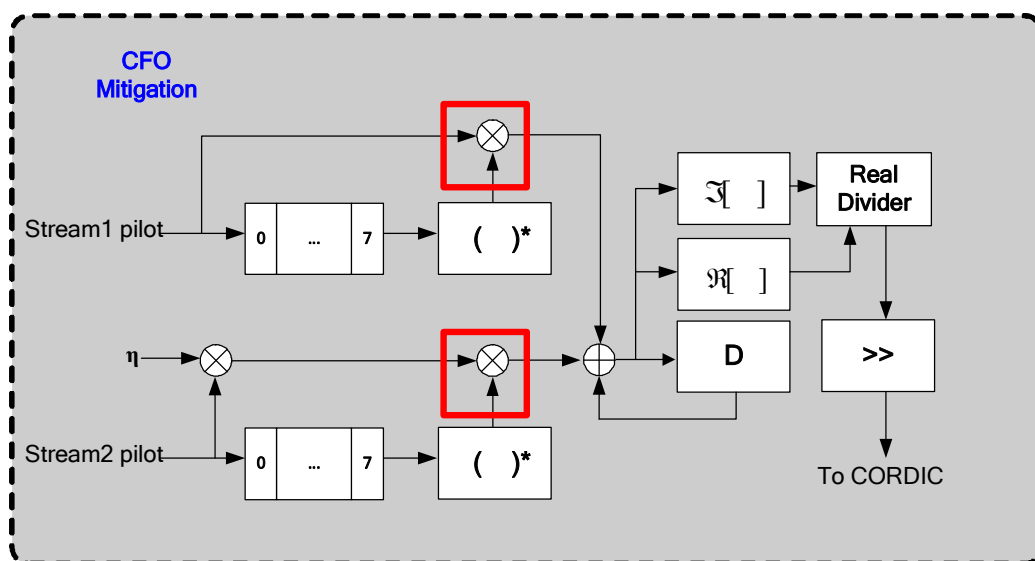


Figure 4.2 The proposed CFO mitigation architecture

The proposed CFO algorithm has the main advantage of low complexity as mentioned in chapter 2. To further reduce the area consumption, we note a feature that CFO mitigation operates during receiving preambles and PET and MIMO detection work during receiving data portion. For this reason, all the main components i.e. the two marked complex multipliers and the real divider shown in Fig.4.2 can share the hardware resources with MIMO detection and PET respectively, so it achieves very low complexity in hardware.

4.2.2 Channel Estimation Module Design

Fig. 4.3 shows the architecture of the proposed tri-mode channel estimation.

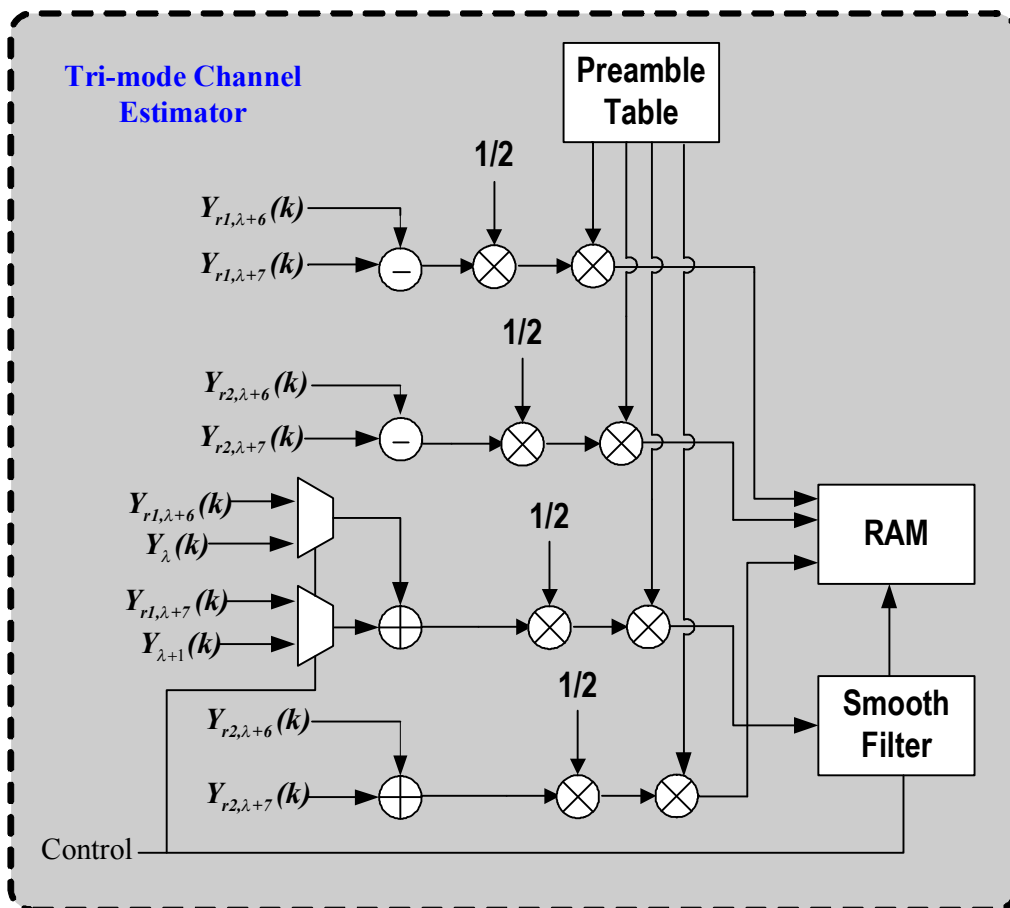


Figure 4.3 Tri-mode architecture of channel estimator

The algorithms of channel estimation were introduced in chapter 2. We observe

that the operation in Equation (2.9) can be totally included in Equation (2.13) so shared architectures of channel estimation is used for three modes. The estimated channel frequency response (CFR) is then sent to a smoothing FIR filter with three taps [0.25 0.5 0.25] for SISO mode, or is saved to RAM without smoothing for SDM-MIMO and STBC-MIMO modes on the other hand.

4.2.3 Phase Error Tracking Module Design

The proposed architecture of CFO tracking is shown as Fig. 4.4. Same as the steps of the proposed algorithm mentioned in chapter 2, we divide the architecture to three portions, i.e. pilot pre-compensation, phase estimation and recursive adjustment. In the pilot pre-compensation portion, the phases of pilots in both data streams are compensated using CORDIC modules. After pilot pre-compensation, the detected pilot phase is the difference between two adjacent OFDM symbols. In the phase estimation portion, the architectures of the weighted average phase estimation for SISO mode and the mean average phase estimation for SDM-MIMO/STBC-MIMO modes are combined together. In addition to mean average phase estimation, there are only two de-multiplexers are addition to the proposed architecture. Most of the components are shared, so this architecture increases little complexity in hardware. Finally, in the recursive adjustment, error vector at current symbol is calculated and the estimated residual CFO is updated. Using the relationship mentioned in equation (2.26), the estimate of SCO can be obtained from CFO. Then the total phase error is sent back to pilot pre-compensation for next symbol duration and is sent to CORDIC modules outside to correct phase errors in data portion.

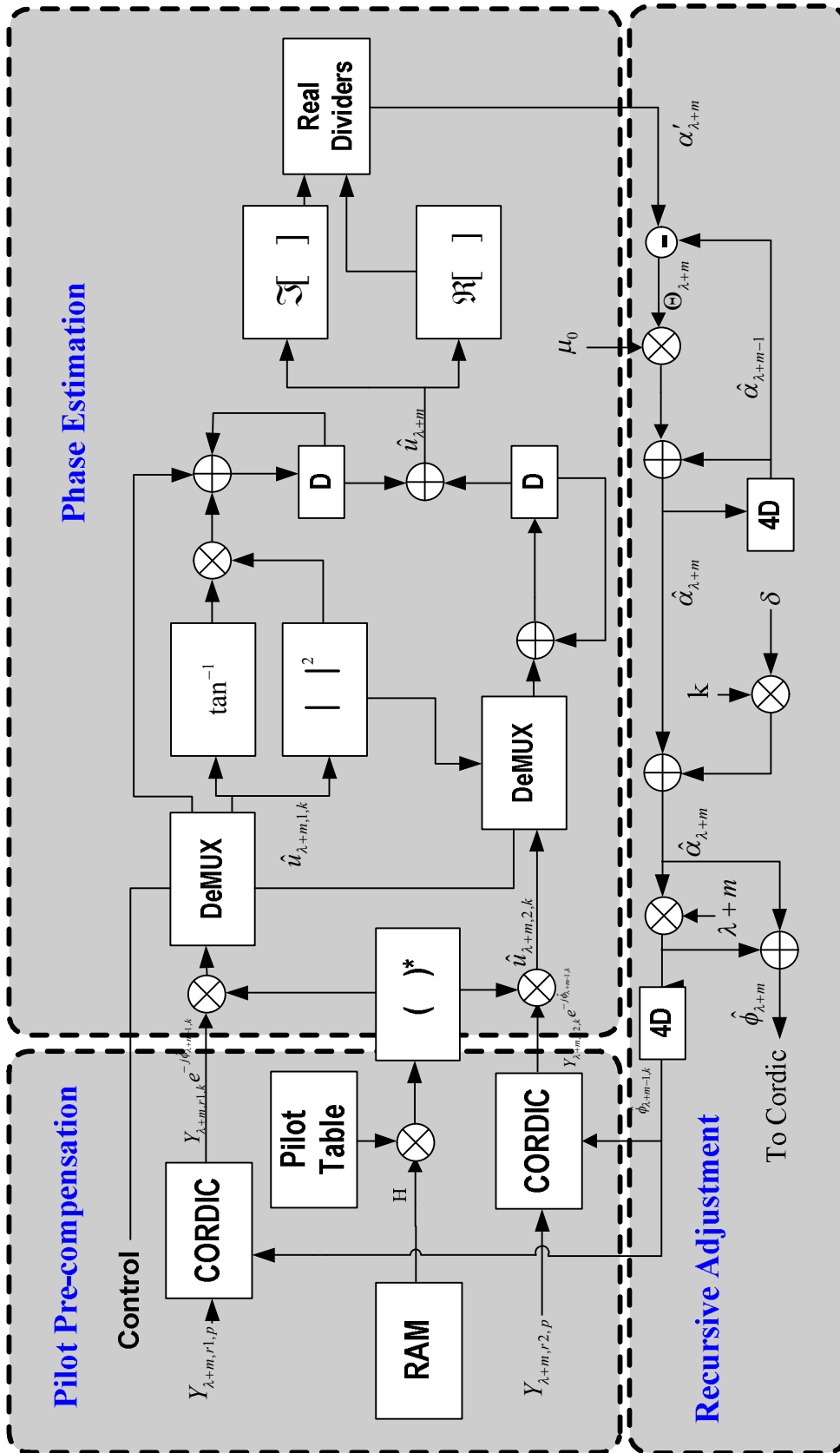


Figure 4.4 The proposed Tri-mode CFO tracker architecture

4.2.4 MIMO Detection Module Design

The channel matrix coefficients of the k -th subcarrier are given by:

$$H_k = \begin{pmatrix} h_{1,k} & h_{3,k} \\ h_{2,k} & h_{4,k} \end{pmatrix} \quad (4.1)$$

It operates under the same subcarrier in the following, so we let $h_{m,k}=h_m$, $H_k=H$. The Equation (4.1) can be re-written as:

$$H = \begin{pmatrix} h_1 & h_3 \\ h_2 & h_4 \end{pmatrix} \quad (4.2)$$

From Equation (2.37), the MMSE filter for SDM-MIMO is:

$$G = H \left[H^H H + \frac{1}{\text{SNR}} I_{N_r \times N_r} \right]^{-1} \quad (4.3)$$

We can re-write Equation (4.3) as

$$G^H = \frac{1}{g} \left\{ \begin{pmatrix} h_1^*(h_4^*h_4) - h_4(h_3^*h_2^*) & h_2^*(h_3^*h_3) - h_3(h_1^*h_4^*) \\ h_3^*(h_2^*h_2) - h_2(h_1^*h_4^*) & h_4^*(h_1^*h_1) - h_1(h_3^*h_2^*) \end{pmatrix} + \alpha \begin{pmatrix} h_1^* & h_2^* \\ h_3^* & h_4^* \end{pmatrix} \right\} \quad (4.4)$$

$$g = (h_1^*h_1)(h_4^*h_4) + (h_2^*h_2)(h_3^*h_3) - (h_1^*h_4^*)(h_2h_3) - (h_2^*h_3^*)(h_1h_4) + \alpha(h_1^*h_1 + h_2^*h_2 + h_3^*h_3 + h_4^*h_4) + \alpha^2 \quad (4.5)$$

where α is the reciprocal of SNR per receiver, and we ignore the effect of α^2

because it is relatively small. The output after MMSE filter can be written as

$$\hat{X}(k) = G^H \cdot Y(k) \quad (4.6)$$

In SISO mode transmission, all the channel frequency responses of h_2 , h_3 and h_4 are zeros. We observe Equation (4.5) can be simplified as zero forcing for SISO mode

$$\hat{X}(k) = \frac{Y(k)}{h_1} \quad (4.7)$$

On the other hand, STBC detection for STBC-MIMO can be expressed as

$$(|h_1|^2 + |h_2|^2 + |h_3|^2 + |h_4|^2) \begin{pmatrix} s_0 \\ s_1 \end{pmatrix} = \begin{pmatrix} h_1^* & h_3 \\ h_3^* & -h_1 \end{pmatrix} \begin{pmatrix} y_0^0 \\ y_0^{1*} \end{pmatrix} + \begin{pmatrix} h_2^* & h_4 \\ h_4^* & -h_2 \end{pmatrix} \begin{pmatrix} y_1^0 \\ y_1^{1*} \end{pmatrix} + N \quad (4.8)$$

The output of STBC detection can be written as

$$\hat{X} = \begin{pmatrix} \hat{x}_0 \\ \hat{x}_1 \end{pmatrix} = \frac{1}{(|h_1|^2 + |h_2|^2 + |h_3|^2 + |h_4|^2)} \left\{ \begin{pmatrix} h_1^* & h_3 \\ h_3^* & -h_1 \end{pmatrix} \begin{pmatrix} y_0^0 \\ y_0^{1*} \end{pmatrix} + \begin{pmatrix} h_2^* & h_4 \\ h_4^* & -h_2 \end{pmatrix} \begin{pmatrix} y_1^0 \\ y_1^{1*} \end{pmatrix} \right\} \quad (4.9)$$

From above derivation, we can find some similarity between MMSE detection and STBC detection. Both detections need channel coefficients $|h_1|^2 + |h_2|^2 + |h_3|^2 + |h_4|^2$, and 2x2 matrix multiplications are required. From above observations, the proposed tri-mode MIMO detection is shown as Fig. 4.5.

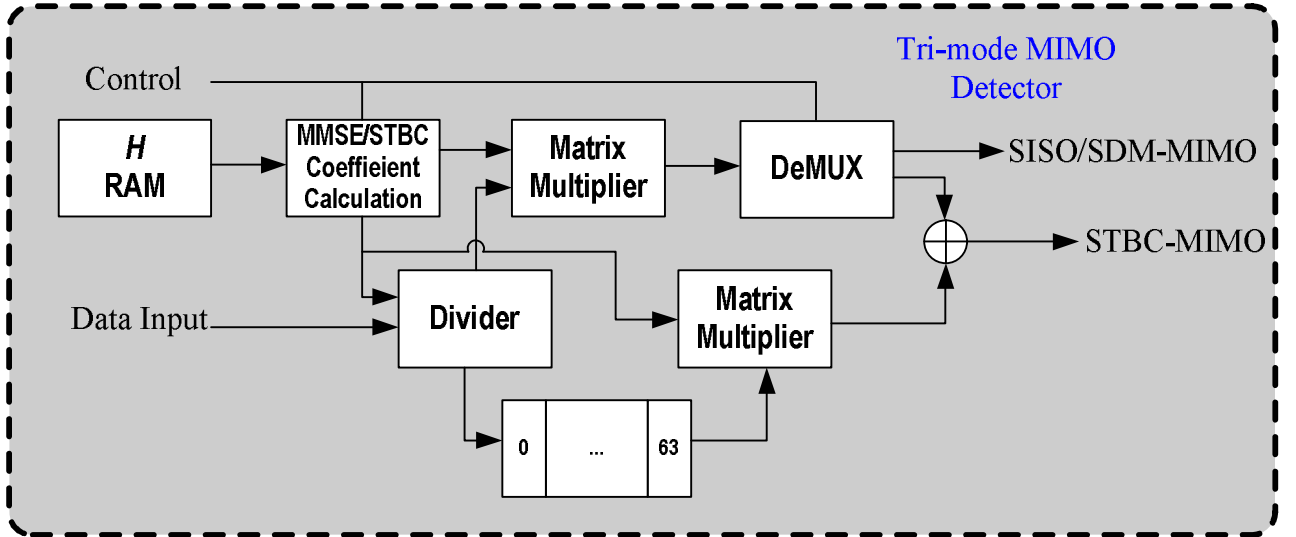


Figure 4.5 Tri-mode MIMO Detector architecture

While designing the proposed architecture, we notice that the channel coefficients $|h_1|^2 + |h_2|^2 + |h_3|^2 + |h_4|^2$ and matrix multiplier can be shared in hardware. The coefficients which MMSE and STBC need are calculated first at the beginning, and then are sent to divider and matrix multipliers. The incoming data are first divided by g as given in Equation (4.5), and then pass through matrix multiplier for SISO and SDM-MIMO modes. In STBC-MIMO mode, some additional operations are need

while receiving. Data is encoded across symbols so a delay line is needed to save data of last symbol. An extra matrix multiplier and an adder are also needed for 2x2 STBC operations in ML MIMO detection. To further reduce the complexity in hardware, we note that there is only one operation in MMSE/STBC coefficients calculation during a packet length so the additional matrix multiplier (lower position in the Fig. 4.5) can share complex multipliers with coefficients calculation block for STBC-MIMO mode.

4.2.5 CORDIC Module Design

CORDIC is used for phase rotation in the proposed architecture. General methods to realize this function needs LUTs, complex multipliers. CORDIC reduces complexity in hardware by usage of simple components like adders, comparators and shifters. CORDIC has another advantage that it can be implemented with pipeline structure easily because of its similar operation in each stage. The i -th iterative formula is defined as

$$\begin{bmatrix} x(i+1) \\ y(i+1) \end{bmatrix} = \begin{bmatrix} 1 & u_i 2^{-i} \\ -u_i 2^{-i} & 1 \end{bmatrix} \begin{bmatrix} x(i) \\ y(i) \end{bmatrix} \quad (4.10)$$

with

$$\theta_i = \tan^{-1}(2^{-i}) \quad (4.11)$$

where the number of stage $i=0,1,2,\dots,N-1$, $[x_i \ y_i]^T$ is the input vector, $[x_{i+1} \ y_{i+1}]^T$ is the output vector, and u_i is use to determine the direction of rotation and is given by

$$u_i = -\text{sign}[z(i)] \quad (4.12)$$

where $z(i)$ is the phase rotated in i -th stage. After finishing the rotation of N stages, the output vector need to be multiplied by the factor

$$A_N = \frac{1}{\prod_{i=0}^{N-1} \sqrt{1^2 + (2^{-i})^2}} \quad (4.13)$$

to maintain the same amplitude as input vector. The CORDIC cell structure of i -th stage is illustrated as Fig. 4.6.

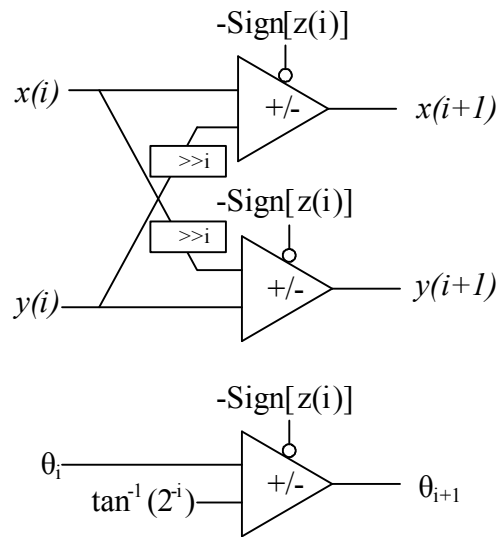


Figure 4.6 The architecture of CORDIC cell at i -th stage

The overall architecture of CORDIC is shown as Fig. 4.7

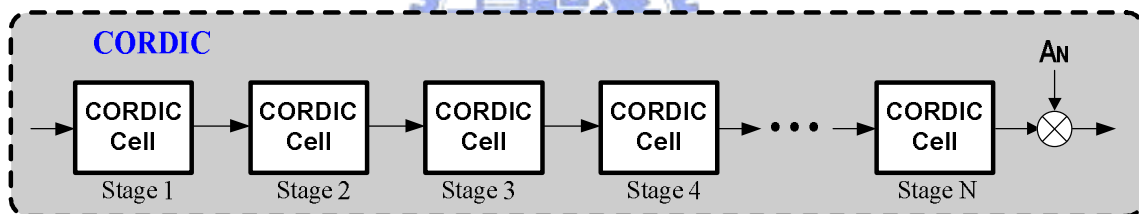


Figure 4.7 The architecture of CORDIC module

While implementing CORDIC, there are issues should be considered. The phase range of the input angle should be between $-\pi \sim \pi$, or errors will occur. Another issue is that the angle value between $-\pi \sim \pi$ is hard to be expressed in 2's complement form. Also, the angular adder can not be implemented by conventional adder and should be redesign. In the proposed design, the input angle of CORDIC is normalized with the factor $2/\pi$, so the range of the phase will be normalized from -2 to 2.

The angle after normalizing is as shown in Fig. 4.8. It shows that the phases can be easily represented as 2's complement form. The most important of all, overflow

issue can be completely solved in this method. For example, the conventional calculation result of $\pi/2 + 3\pi/4 = 5\pi/4$ ($= -3\pi/4$), the proposed calculation result obtains result of $01.0_{(2)} + 01.1_{(2)} = 10.1_{(2)}$ correctly.

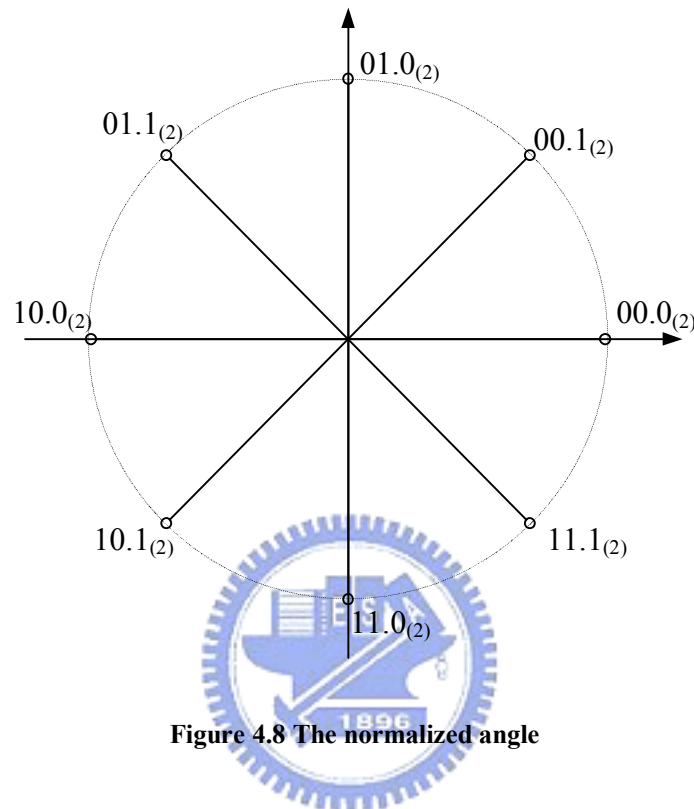


Figure 4.8 The normalized angle

4.3 Implementation Results

4.3.1 Fixed-point Simulation

Before developing RTL code, we have to determine the bit numbers of each operation. To reduce hardware complexity, fewer bit numbers are better. However, hardware cost and system performance are trade-off in hardware implementation. The bit numbers of main modules in tri-mode equalizer are listed in Table 4.1.

After the bit numbers of each operation are determined, fixed-point simulation are utilized to evaluate the system performance in hardware. The performance comparison of floating point and fixed point simulations in the highest data rate condition of 64QAM and 5/6 coding rate under TGN channel model D, 40ppm CFO

and 40ppm SCO for 2x2 SDM-MIMO are shown as Fig. 4.9. We can note that in Fig. 4.9, there is only 0.3 dB performance loss in fixed-point simulation compared with floating point simulation.

Table 4.1 Bit numbers of main modules

Module Name	Bit Numbers
CFO Mitigation Input	16
Channel Estimation Input	11
PET Input	16
MIMO Detection Input	11
CORDIC Input	13
CORDIC Output	16

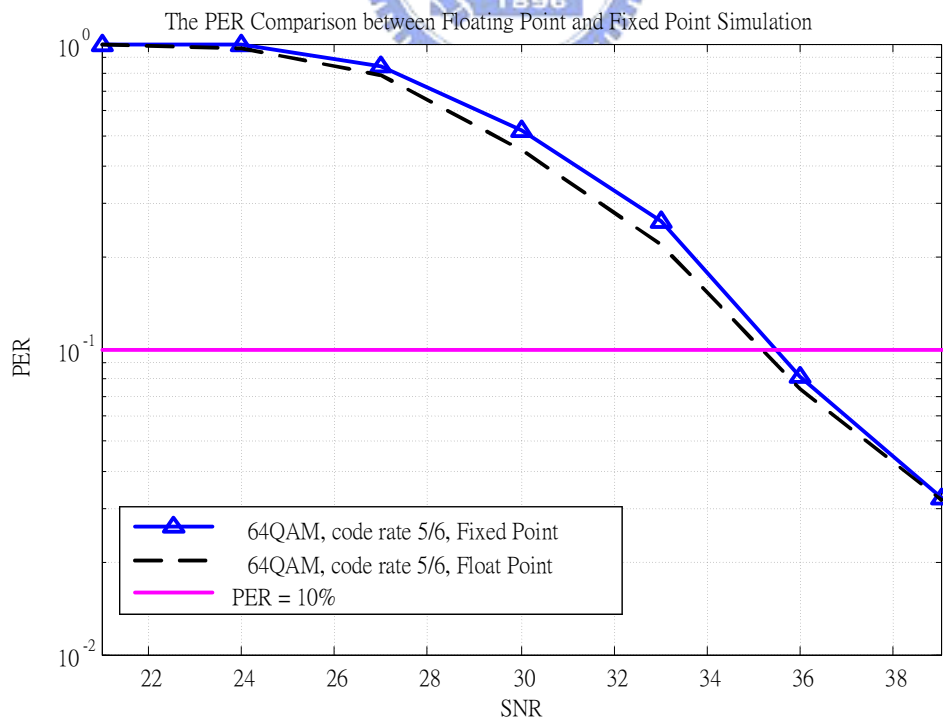


Figure 4.9 Performance comparisons between floating point and fixed point simulation.

4.3.2 Hardware Synthesis

In this section, we discuss the implementation of the proposed tri-mode equalizer design. We use SYNOPSIS Design Compiler to synthesize the register-level verilog file in a UMC 0.18 μ m cell library with 20MHz clock rate. The Hardware complexity of the tri-mode equalizer is shown in Table 4.2.

Table 4.2 Hardware complexity of the tri-mode equalizer

Main Block	Gate Count	Memory Size (Bytes)
Mitigation	8k	0
Channel Estimation	6k	4.5
CORDIC * 2	16k	0
PET	37k	0
MIMO Detection	116k	2.75
Total	209k	7.25

From Table 4.2, the total gate counts of the tri-mode equalizer are 209k, and it occupies 7.25 Bytes of memory. The proposed tri-mode MIMO detection which occupies highest percentage in area in the tri-mode equalizer is compared with former approaches as listed in Table 4.3.

Table 4.3 Gate count comparison for 2x2 MIMO symbol detectors

	Mode	Gate Count
[21]	SISO	60K
[22]	SDM	89K ¹
[24]	SDM / SFBC	128K
This Work	SDM / STBC / SISO	116K

¹ This value is the scaled gate count value of [22]. The scaling factors are defined in [23].

In order to analyze whether the proposed design meets the timing requirement in 802.11n, timing report is shown as:

```

*****
Report : timing
    -path full
    -delay max
    -max_paths 1
Design : TOP
Version: W-2004.12
Date   : Tue May 13 22:51:53 2008
*****
Operating Conditions: slow   Library: slow
Wire Load Model Mode: top

Startpoint: I_CFO_MITIGATION/counter_reg[5]
            (rising edge-triggered flip-flop clocked by clock)
Endpoint:  COMPENSATE2_CORDIC/out_x_reg[15]
            (rising edge-triggered flip-flop clocked by clock)
Path Group: clock
Path Type: max

```

clock clock (rise edge)	50.00	50.00
clock network delay (ideal)	0.00	50.00
COMPENSATE2_CORDIC/out_x_reg[15]/CK (EDFFXL)	0.00	50.00 r
library setup time	-0.43	49.57
data required time		49.57

data required time		49.57
data arrival time		-49.57

slack (MET)		

From timing report, the critical path exists from the counter in the CFO mitigation module to CORDIC module. The system timing constraint is 50ns, library setup time is 0.43ns and data required time of critical path is 49.57ns, so timing of the proposed design meets system requirements.

Device Utilization Summary				
Logic Utilization	Used	Available	Utilization	Note(s)
Number of Slice Flip Flops	10,196	53,248	19%	
Number of 4 input LUTs	31,029	53,248	58%	
Logic Distribution				
Number of occupied Slices	21,316	26,624	80%	
Number of Slices containing only related logic	21,316	21,316	100%	
Number of Slices containing unrelated logic	0	21,316	0%	
Total Number 4 input LUTs	31,668	53,248	59%	
Number used as logic	31,029			
Number used as a route-thru	639			
Number of bonded IOBs	102	640	15%	
Number of BUFG/BUFGCTRLs	1	32	3%	
Number used as BUFGs	1			
Number used as BUFGCTRLs	0			
Total equivalent gate count for design	407,517			
Additional JTAG gate count for IOBs	4,896			

Figure 4.10 The synthesis report of tri-mode equalizer on ISE

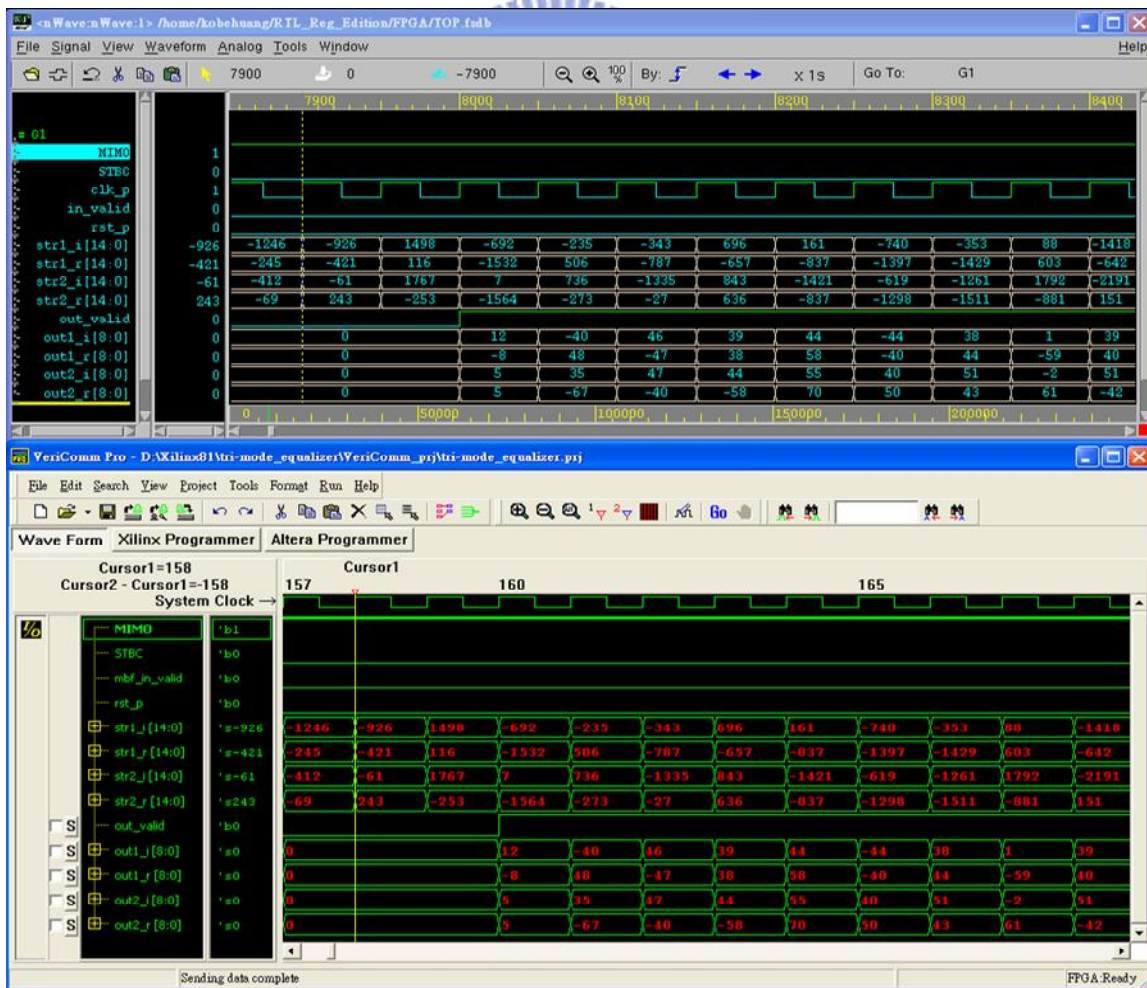


Figure 4.11 Comparison of RTL simulation and FPGA emulation.

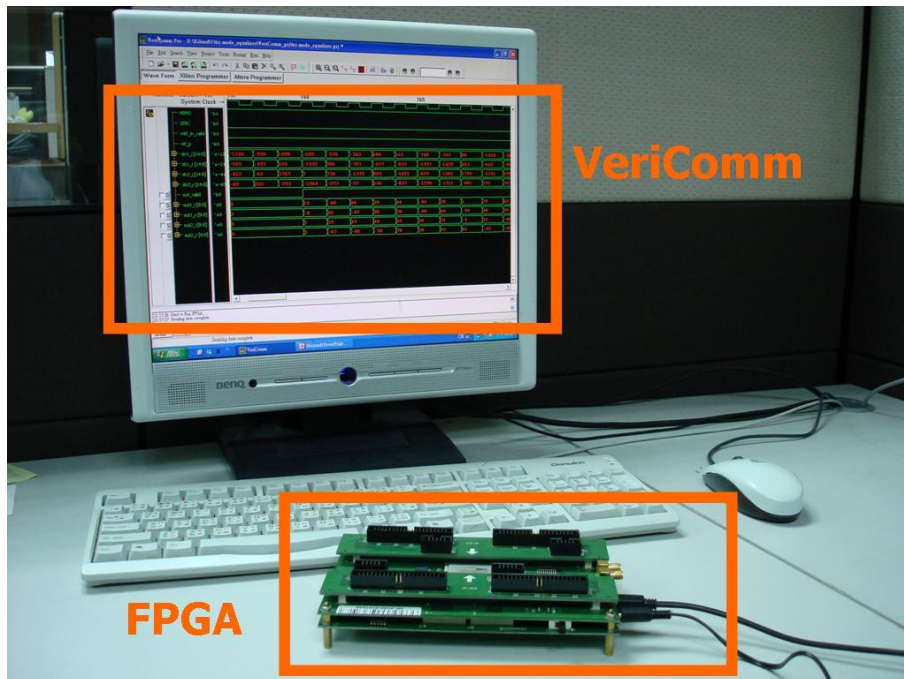


Figure 4.12 VeriComm and FPGA board

For FPGA verification, the tri-mode equalizer is also synthesized by XST Synthesizer built in Xilinx ISE, the synthesis report is show as Fig 4.10.

Finally, to verify the functional correctness on FPGA, the comparisons of the simulation results of RTL on nWave and emulation results of FPGA on VeriComm are shown in Fig 4.11. Fig. 4.12 depicts the verifying situation. We claim that their behaviors are correct from Fig 4.11 because the outputs are totally identical as inputting the same patterns.

Chapter 5

Conclusions and Future Works

In this thesis, we proposed a tri-mode equalizer design which can operate in SISO/SDM-MIMO/STBC-MIMO for IEEE 802.11n draft. The architecture of tri-mode equalizer is divided to four portions: CFO mitigation, channel estimation, phase error tracking and MIMO detection. In CFO mitigation, the proposed algorithm increases the accuracy of channel estimation effectively and has low complexity in hardware. Zero Forcing channel estimation for SISO mode can be fully integrated into MIMO channel estimation for SDM-MIMO/STBC-MIMO modes in the proposed architecture, so shared-architecture leads to low area consumption for tri-mode channel estimator. In the proposed PET, a full tracking range can be achieved by the pilot pre-compensation scheme, the performance degradation of conventional pilot-based PET due to few pilot numbers can be improved outstandingly, and shared architectures are also considered in the proposed circuit. Finally, Zero Forcing equalization for SISO mode, MMSE MIMO symbol detection for SDM-MIMO mode and ML MIMO symbol detection for STBC-MIMO mode are implemented with a lot of shared architectures to reduce area consumption in circuit. Simulation results show the proposed tri-mode equalizer achieves a better 1.9~3.8dB gain in SNR for 10% PER compared with conventional approaches because a total solution of residual CFO are proposed. In hardware implementation, totally 209k gate counts are used for tri-mode equalizer. Low area consumption in the proposed circuit design is achieved by using a lot of shared architectures.

In this thesis, we focus on equalizer design for 2x2 MIMO systems. Using this design concept, a tri-mode inner receiver can also be considered in the future. For higher data rate and higher reliability transmission, a MIMO system with higher antenna dimensions will be certainly applied in the future. Therefore, an MIMO equalizer in the high throughput transmission with more antennas will be needed to further explore in the future.



Bibliography

- [1] S. M. Alamouti, “A simple transmit diversity technique for wireless communications,” *IEEE Journal on Select Areas in Communications*, vol. 16, pp. 1451-1458, Oct. 1998.
- [2] V. Tarokh, H. Jafarkhani, and A. R. Calderbank, “Space-time block codes from orthogonal designs,” *IEEE Trans. Inform. Theory*, vol. 45, pp. 1456–1467, July 1999.
- [3] J. Liu and J. Li, “Parameter estimation and error reduction for OFDM-based WLANs,” *IEEE Trans. Mobile Computing*, vol 3, no 2, pp. 152-163, April-June 2004.
- [4] F. Peng, and J. Zhan, “On Residual Carrier Frequency Offset Mitigation for 802.11N,” in *Proc. ICASSP*, 2007, vol. 3, p. 257-260.
- [5] IEEE 802.11 TGn channel model special committee, “TGn Channel Models for IEEE 802.11 WLANs”, *IEEE doc.: IEEE 802.11-03/940r4*, May 2004.
- [6] A. P. Stephens, “IEEE 802.11 TGn comparison criteria, Tech. Rep. IEEE 802.11-03/814r31, May 2004.
- [7] A.A.M. Saleh and R.A. Valenzuela, “A statistical model for indoor multipath propagation,” *IEEE J. Select. Areas Commun.*, vol. 5, 1987, pp. 128-137.
- [8] Q.H. Spencer, et al., “Modeling the statistical time and angle of arrival characteristics of an indoor environment,” *IEEE J. Select. Areas Commun.*, vol. 18, no. 3, March 2000, pp. 347-360.
- [9] R.J-M. Cramer, R.A. Scholtz, and M.Z. Win, “Evaluation of an ultra-wide-band propagation channel,” *IEEE Trans. Antennas Propagat.*, vol. 50, no.5, May 2002, pp. 561-570.
- [10] Chia-Chin Chong, David I. Laurenson and Stephen McLaughlin, “Statistical Characterization of the 5.2 GHz wideband directional indoor propagation channels with clustering and correlation properties,” in *proc. IEEE Veh. Technol.*

Conf., vol. 1, Sept. 2002, pp. 629-633.

- [11] L. Schumacher, K. I. Pedersen, and P.E. Mogensen, "From antenna spacings to theoretical capacities – guidelines for simulating MIMO systems," in *Proc. PIMRC Conf.*, vol. 2, Sept. 2002, pp. 587-592.
- [12] L. Schumacher "WLAN MIMO Channel Matlab program," download information:
http://www.info.fundp.ac.be/~lsc/Research/IEEE_80211_HTSG_CMSC/distribution_terms.html
- [13] IEEE 802.11 working group, *IEEE P802.11n/D0.02*, Feb 2006.
- [14] Shou-Yin Liu, long-Wha Chong, "A study of joint tracking algorithms of carrier frequency offset and sampling clock offset for OFDM-based WLANs", Communications, Circuit and System and West Sino Expositions. IEEE International Conference, vol. I, pp. 109-113, July. 2002.
- [15] *Wireless LAN Medium Access Control (MAC) and Physical Layer (PHY) Specifications: High Speed Physical Layer (PHY) in the 5 GHz Band*, IEEE Standard 802.11a, 1999.
- [16] Y.H. Yu, H.Y. Liu, T.Y. Hsu, and C.Y. Lee, "A Joint Scheme of Decision-Directed Channel Estimation and Weighted-Average Phase Error Tracking for OFDM WLAN Systems", in *Proc. APCCAS*, 2004, vol. 2, pp. 629-633
- [17] P. Y. Tsai, H. Y. Kang, and T. D. Chiueh, "Joint weighted least squares estimation of frequency and timing offset for OFDM systems over fading channels," in *Proc. IEEE VTC'03*, Cheju, Korea, Apr. 2003, pp. 2543–2547.
- [18] A. V. Zeist "Space Division Multiplexing algorithms," *10th Mediter-ranean Electrotechnical Conference*, vol.3, 2000.
- [19] Joint Proposal Team PHY Simulation Results: IEEE 802.11-06/0067r02
- [20] I-Tai Lu, Hsin-Chang Wu, Yongwen Yang, Olesen, R.," Carrier Frequency Offset Mitigation in a Proposed MIMO OFDM System," *Systems, Applications and*

Technology Conference, IEEE International Conference, pp. 1-5, May. 2007.

- [21] Chia-Sheng Peng, Yuan-Shin Chuang, Kuei-Ann Wen, "CORDIC-based architecture with channel state information for OFDM baseband receiver," *IEEE Trans. Consumer Electronics*, vol 51, pp. 403-412, May 2005.
- [22] Shingo Yoshizawa and Yoshikazu Miyanaga, "VLSI implementation of high-throughput SISO-OFDM and MIMO-OFDM transceivers," *International Symposium on Communications and Information Technologies (ISCIT)*, No. T2D-4, Oct. 2006.
- [23] Gilbert, J.M., Won-Joon Choi, Qinfang Sun, "MIMO technology for advanced wireless local area networks," in Proc. Design Automation Conference, 2005, pp. 413-415
- [24] Seongjoo Lee, Seungpyo Noh, Yunho Jung, Jaeseok Kim, "Efficient design of symbol detector for MIMO-OFDM based wireless LANs," ICT-MICC, IEEE International Conference, pp. 510-514, May. 2007.



Vita

姓名：黃俊彥

性別：男

籍貫：宜蘭縣

生日：民國七十三年一月二十四日

地址：宜蘭市西後街 131 號

學歷：國立交通大學電子工程研究所碩士班 95/09~97/06

國立中興大學電機工程學系 91/09~95/06

國立宜蘭高級中學 88/09~91/06



論文題目：A Tri-mode MIMO Equalizer Design for OFDM Based Wireless LANs

三模 MIMO 之無線區域網路等化器設計